CZECH TECHNICAL UNIVERSITY IN PRAGUE
Faculty of Nuclear Sciences and Physical Engineering

Ubíhající elektrony a jejich detekce segmentovanými křemíkovými detektory

Runaway electrons and their detection using segmented silicon detectors

Research project

Author: **Bc. Sergei Kulkov**

Supervisor: **Ing. Michal Marčišovský, Ph.D.**

Consultant: **Ing. Peter Švihra**

Academic year: **2018/2019**

ČESKÉ VYSOKÉ UČENÍ TECHNICKÉ V PRAZE
FAKULTA JADERNÁ A FYZIKÁLNĚ INŽENÝRSKÁ
PRAHA 1 - STARÉ MĚSTO, BŘEHOVÁ 7 - PSČ 115 19

Katedra: fyziky **Akademický rok:** 2018/2019

VÝZKUMNÝ ÚKOL

Student: **Bc. Sergei Kulkov**

Studijní program: Aplikace přírodních věd

Obor: **Fyzika a technika termojaderné fuze**

Vedoucí úkolu: Ing. Michal Marčišovský, PhD.

Název úkolu (česky/anglicky):
Ubíhající elektrony a jejich detekce segmentovanými křemíkovými detektory/
Runaway electrons and their detection using segmented silicon detectors

Pokyny pro vypracování:
1. Fyzika termojaderné fúze a metody diagnostiky
2. Ubíhající elektrony (RE), jejich vznik, propagace a mitigace
3. Interakce záření s materiálem relevantní k detekci RE
4. Segmentované polovodičové detektory záření
5. Analýza experimentálních dat získaných na měření na tokamacích

Úkol bude vypracován v anglickém jazyce.

Součástí zadání výzkumného úkolu je jeho uložení na webové stránky katedry fyziky.

Literatura:

1. P. Kulhánek: Úvod do teorie plazmatu, AGA, 2011
2. J. Wesson: TOKAMAKS, Oxford University Press, 2011
3. G. F. Knoll: Radiation Detection and Measurement, Wiley, 2010
4. G. Lutz: Semiconductor Radiation Detectors, Springer, 1999
5. K. Iniewski: Radiation Effects in Semiconductors, CRC Press, 2011
6. Aktuální informace z oboru získané z oborových recenzovaných časopisů

Datum zadání: 22.10.2018

Datum odevzdání: 28.06.2019

....

vedoucí katedry

Acknowledgment

I would like to thank my supervisor Ing. Michal Marcisovsky, Ph.D. for the valuable remarks and engagement through the writing of this research project. Also, I would like to thank Ing. Peter Svihra for the useful comments and contribution that improved this work.

Bc. Sergei Kulkov

Title: **Runaway electrons and their detection using segmented silicon detectors**

Author: Bc. Sergei Kulkov

Specialization: Physics and Technology of Thermonuclear Fusion

Supervisor: Ing. Michal Marcisovsky, Ph.D., Department of Physics, Faculty of Nuclear Sciences and Physical Engineering, Czech Technical University in Prague

Consultant: Ing. Peter Svihra, Department of Physics, Faculty of Nuclear Sciences and Physical Engineering, Czech Technical University in Prague

Abstract: The main goal of this research project is to describe fundamental physics of runaway electrons (RE), mechanisms of their generation, methods of diagnostics, and strategies of mitigation. One of the themes described in this work is the interaction of radiation with matter relevant to RE diagnostics: bremsstrahlung, interaction of photons with material, and generation of photoneutrons. Furthermore, it summarizes properties of semiconductor materials and detectors based on them. The PH32 readout chip and the X-chip-03 detector are described. The latter was tested during a RE campaign at tokamak COMPASS. Basic analysis of the acquired data is presented.

Key words: tokamaks, semiconductor detectors, runaway electrons

Contents

Introduction

Thermonuclear fusion reactions are the primary source of energy in stars. Conditions for the reactions to occur are defined primarily by the mass and elemental composition of the star. Achieving thermonuclear fusion on Earth is possible as well; however, it is much more difficult to reach viable conditions. Fusion in a laboratory can be achieved via two strategies: magnetic confinement fusion and inertial confinement fusion. The first one relies on machines such as tokamaks and stellarators, while the second one founds use in lasers. At present, tokamaks dominate in fusion physics and the first nuclear fusion reactor with net positive energy gain will be based on a tokamak configuration. However, tokamaks and associated technologies still have a lot of difficulties to overcome.

Runaway electrons are high-energy particles that may be generated during tokamak operation. These particles are accelerated by the electric field to relativistic velocities and they may have a negative effect on the machine operation, as they shorten its lifetime. Physics of runaway electrons is not yet fully understood. New diagnostic methods are being developed as well as mitigation strategies to prevent either their generation or the damage they can inflict. Runaway electrons cover a wide spectrum of energies and there is no diagnostic technique, that can measure in the whole energy range.

Recently, plasma diagnostics has found use of the semiconductor detectors, which are widely applied in the high energy physics. Semiconductor detectors have many advantages over other instruments in plasma diagnostics, such as scintillator detectors, inteferometers, and probes. Among them is fast operation, lower energy required to generate charge carriers, and compact size. The latter enables direct measurements, when a detector is installed into the tokamak's first wall. However, such operational conditions make semiconductor detectors more vulnerable to the damage induced by heat and neutron fluxes. The use of semiconductor detectors for plasma diagnostics is a novel technique. It is important to test and adapt the technology to the tokamak's harsh environment, as besides the damaging radiation, electronics is exposed to intense electromagnetic fields.

This work is composed in the following way: the first chapter serves as introduction to plasma physics, since it summarizes basic plasma characteristics and parameters, requirements for thermonuclear fusion in a reactor, and tokamak's general configuration. The second chapter discusses runaway electrons: mechanisms of their generation, methods of diagnostics and mitigation strategies. The third chapter summarizes interactions of radiation with matter that are most important for the runaway electrons diagnostics. The fourth chapter describes fundamental properties of semiconductor materials and detectors, that were recently implemented and tested in tokamak experiments. The fifth chapter summarizes the results of the measurements conducted with strip semiconductor detectors in tokamaks GOLEM and COMPASS.

1 Physics of thermonuclear fusion

A nuclear fusion reaction is a reaction in which two or more atomic nuclei are combined forming a different heavier nucleus. In such a reaction, energy is released. This is possible due to the difference in masses of the reactants and the products. This difference is a measure of the nuclear binding energy, which is the energy required to remove a nucleon from the nucleus of an atom. Binding energy ΔE and the mass difference Δm are bound by the Einstein relation [1]:

$$\Delta E = \Delta m c^2 \tag{1}$$

Figure 1 shows the dependence of binding energy per nucleon on the mass number. The curve is divided into two sections (relatively to ^{56}Fe): heavier nuclei can undergo fission reaction and lighter nuclei can undergo fusion reaction. Both reactions yield energy given by equation (1).

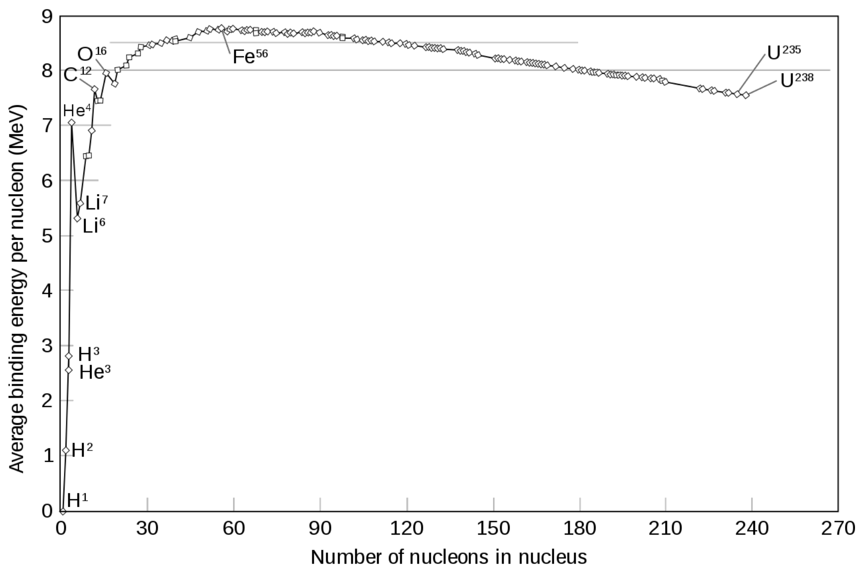

Figure 1: Binding energy per nucleon. The peak is reached for ^{56}Fe, that divides the curve into two parts. Elements with lower atomic number may undergo fusion nuclear reactions, heavier elements may undergo fission reactions. A local maximum on the fusion part of the curve is represented by ^{4}He [2].

An example of a fusion reaction is the so-called "deuterium-tritium (D-T) reaction":

$$D + T \rightarrow {}^4He + n + 17.59 \text{ MeV}, \tag{2}$$

where D is a nucleus of deuterium and T is a nucleus of tritium. Energy yield is released in the form of the kinetic energy of the products. For a nuclear fusion reaction to occur, ions need to penetrate the Coulomb barrier given by the repulsive force due to the positive charge of both ions. One way to achieve that is by high temperatures. Temperature is a measure of the average kinetic energy of particles, so high temperature particles gain high kinetic energies, and if that energy is sufficient for ions to penetrate the Coulomb barrier, the nuclei undergo thermonuclear fusion reaction.

1.1 Plasma

Plasma is the most common state of the atomic matter in the Universe. Stars, interstellar gasses and clouds, solar winds and the ionosphere of Earth are composed of plasma. The term "plasma" is used for ionized gas and it was introduced by the American physicist and chemist Irving Langmuir in his article in 1928 [3] because of the similarity between the highly ionized gas and the blood plasma. Plasma has three key characteristics [4]:

- Plasma has free charge carriers (free electrons and ions);
- In plasma, ion and electron densities are equal (quasi-neutrality);
- Plasma responds to the electric and magnetic fields as a whole and it also generates those fields by itself.

The key parameters of the plasma are ion and electron temperature $T_{\mathrm{i,e}}$ and density $n_{\mathrm{i,e}}$. Because it is composed of free charged particles, plasma can interact with acoustic and electromagnetic waves, which have a lot of different modes in plasma. In plasma physics, there are several approaches to describe plasma: the first one is the statistical physics approach to analyze transport, relaxation, micro-instabilities, and the Landau damping effect, the second one is the magnetohydrodynamics (MHD) that describes plasma-wave interaction and macro-instabilities [4].

Charged particles put in the magnetic field become confined. Electrons and ions undergo Larmor rotation in circles with the radius (Larmor radius) and angular frequency given by:

$$R_{\mathrm{L}} \equiv \frac{mv_{\perp}}{|Q|B}, \qquad \omega_{\mathrm{c}} \equiv \frac{|Q|B}{m}, \tag{3}$$

where m is the mass of the particle, $v_{\perp}$ is the component of the particles velocity perpendicular to the magnetic field B, Q is the charge of the particle. If the particle has also a component of velocity in the direction of the magnetic field, the resulting shape of the trajectory would be a helix shown in Figure 2.

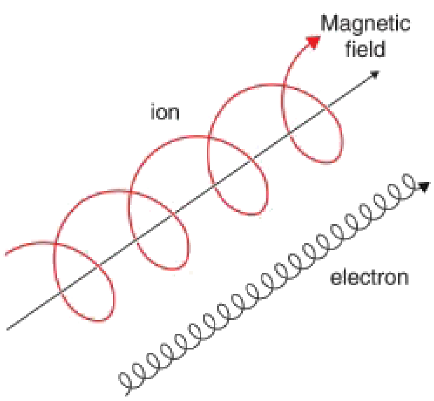

Figure 2: Helical trajectory of ions and electrons in a homogeneous magnetic field. The direction is clockwise for ions and counterclockwise for electrons given by the charge.

The possibility of trapping plasma particles in a magnetic field is crucial for the so-called magnetic confinement fusion, which will be discussed later in chapter 1.3.

Other important plasma parameters will be used in equations in the next chapters. The first one is the *Debye length*. Consider a negative and positive charge put into plasma. Due to the Coulomb interaction between the charges and the bulk plasma particles, the positive charge will attract electrons from the plasma and repel positive ions and vice versa for the negative charge. Each one of the charges will become screened by the particles with the opposite charge, forming the so-called *Debye spheres*. This state of plasma is schematically shown in Figure 3.

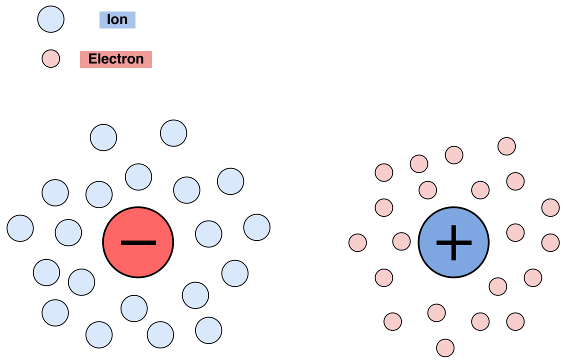

Figure 3: The Debye sphere. Charges put into plasma become screened by particles with opposite charges.

The radius of a Debye sphere is given by the *Debye length*, which is a measure of plasma screening. It was shown, that both positive and negative charges are screened in plasma [5]. However, for the Debye length derivation, only electrons are taken into consideration, because they have much higher mobility than ions and they react much faster to charge fluctuations in plasma. The Debye length is then given by [5]:

$$\lambda_{\mathrm{D}} \equiv \left(\frac{\varepsilon_0 \mathrm{k_B} T_{\mathrm{e}}}{n_{\mathrm{e}} \mathrm{e}^2}\right)^{\frac{1}{2}}, \tag{4}$$

where ε_0 is the vacuum permittivity constant, $\mathrm{k_B}$ is the Boltzmann constant, T_{e} is the electron temperature, n_{e} is density of electrons in plasma and e is the electron charge. Debye length gives another explanation of the quasi-neutrality of plasma: if the size of the system which contains plasma is much larger than the Debye length, then the bulk plasma contains no electric potentials as they are all screened. In other words, it is impossible to distinguish between positive and negative charges in different regions of plasma; nonetheless, plasma interacts with electromagnetic fields.

Another important parameter b_0 is connected with the Rutherford equation for Coulomb interactions. Consider a Coulomb interaction between two particles with charges of the same sign. A so-called *collision parameter* is a distance between the initial path of the incident particle and a parallel line to this path drawn through the second particle. For the distance $b = b_0$ the incident particle will repel at an angle of 90°. The meaning of the parameter b_0 is shown schematically in Figure 4.

The b_0 parameter is defined [4]:

$$b_0 \equiv \frac{Q_\alpha Q_\beta}{4\pi\varepsilon_0 \mu g^2}, \; \mu \equiv \frac{m_\alpha m_\beta}{m_\alpha + m_\beta}, \; g \equiv |\boldsymbol{v}_\alpha - \boldsymbol{v}_\beta|. \tag{5}$$

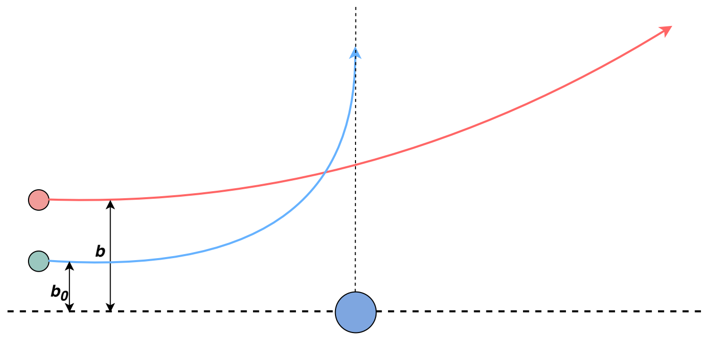

Figure 4: Coulomb interaction between two particles with charges of the same sign. Parameter b is the collision parameter, b_0 is the critical collision parameter for scattering at a 90° angle.

Another parameter that will be used further in equations is the so-called *Coulomb logarithm*, which is defined:

$$\ln \Lambda \equiv \ln \left(\frac{\lambda_D}{b_0} \right). \tag{6}$$

When collisions are considered in plasma, they are usually taken with bounds given by b_0, which acts as the lower limit for collisions with scattering at an angle of 90°, and by λ_D, which acts as the upper limit for collisions with scattering at small angles. The Coulomb logarithm is a measure of how the small-angle collisions are more effective than the large-angle collisions.

1.2 Thermonuclear fusion reactions in stars

Stars in the main sequence are made of hot plasma which is held together by the force of gravity given by the mass of the star. Fusion reactions in stars are their main source of energy and they also define the life cycle of stars. High temperature and pressure create a favorable environment for nuclear fusion reactions which convert hydrogen atoms (or protons) into helium atoms through a multistage process known as the proton-proton (PP) cycle shown in Figure 5.

The PP cycle takes place in stars with a mass $< 1.3\ M_\odot$, where $M_\odot$ is the mass of the Sun. The other branch of nuclear fusion reactions is the CNO cycle which involves carbon, nitrogen, and oxygen acting as catalysts in the reaction. However, this process demands, that these elements are already present in the star. Products of the PP cycle, atoms of ^{4}He, may fuse with each other or with an atom of H producing ^{8}Be. This element is unstable with half-life of 8.19×10^{-17} s. However, an atom of ^{8}Be may interact with another atom of ^{4}He producing carbon. When atoms of H are completely burnt, the star begins to contract and heat up. In these conditions, alpha particles can fuse fast enough to produce carbon. This process is known as the *three-alpha process*. During this chain of nuclear fusion reactions, an atom of carbon can fuse with an atom of helium producing ^{16}O. Nitrogen can be produced via fusion reactions between carbon and hydrogen. This branch dominates in the stars with a mass $\geq 1.3\ M_\odot$ [7].

The first who named nuclear fusion as the source of energy in stars was English physicist and astronomer Arthur Eddington. Later, German-American physicist Hans Bethe described the PP and CNO cycle in stars in his article in 1939 [8]. For this work and generally for the contribution to the theory of nuclear reactions he was awarded the Nobel Prize in physics in 1967 [9].

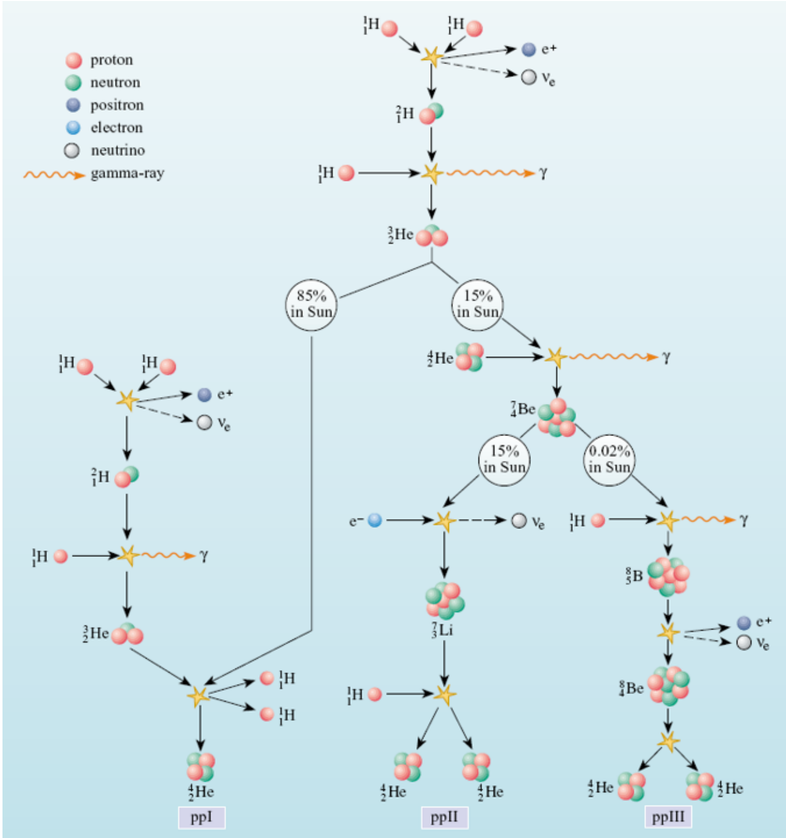

Figure 5: The so-called proton-proton cycle of nuclear fusion reactions which is a dominant source of energy in stars with mass $< 1.3M_{\odot}$ [6].

1.3 Thermonuclear fusion reactions on Earth

As stars get energy from the nuclear fusion reaction, it was shown in mid-20$^{\text{th}}$ century, that fusion is also possible on Earth. While plasma in stars is confined by the force of gravity, there are other approaches to make fusion reactions possible in a laboratory such as the magnetic confinement fusion (MCF) and the inertial confinement fusion (ICF).

In the MCF, the key role belongs to the force of the magnetic field in which particles become trapped. With the use of different external sources of heat such as electric current, electromagnetic waves, and neutral particles [10], MCF can achieve conditions necessary for nuclear fusion reactions to occur. There are different approaches in the MCF that are being tested. Two particular ones are tokamaks, which will be discussed in the next chapter, and stellarators [11]. Both tokamaks and stellarators act as a confinement chamber for hot plasma using an external magnetic field. The main difference between the two is that in tokamaks there is an electric current driven through the plasma. Both machines have their advantages and disadvantages [12].

The ICF approach in one of its strategies uses lasers to compress small fuel pellets to initiate a nuclear fusion reaction. Energy is delivered to the outer layers of the pellet, which then ablates, producing a force that accelerates the inner layers inwards, compressing and heating the fuel (usually deuterium-tritium gas) to the required conditions for fusion reactions. This approach in the ICF known as direst.

However, the pellet can be also compressed indirectly. In this approach, the pellet is kept inside a metallic cylinder (typically gold-plated cylinder) known as *hohlraum*. Energy is delivered onto the cylinder, where it is absorbed ,leading to the emission of X-rays that afterwords compress the pellet.

Confinement in a laboratory is a question of balance. In the MCF, while there is energy yield from the fusion reactions, there is also a loss of energy at play due to radiation - the *bremsstrahlung effect*, which is the emission of a photon during the scattering of an electron from an atom [13]. In order to initiate a fusion reaction, it is mandatory to achieve high temperatures and high densities. The drawback is that bremsstrahlung also increases at higher temperatures and densities [14]. For energy gains to balance the energy losses, it is required to confine the reactions long enough. This is described by the energy *confinement time* τ parameter. It is defined as the ratio of the whole thermal energy stored in plasma to the power losses:

$$\tau \equiv \frac{W_{\mathrm{p}}}{P_{\mathrm{L}}}. \tag{7}$$

In other words, confinement time is the characteristic time during which the energy remains in plasma before escaping. Through out the course of fusion research, confinement time values of the order up to 1 second in the tokamak JET were achieved [15].

With the right set of temperature T, density n and confinement time τ, it is possible to achieve ignition of plasma, which is the state in confinement configuration when the losses are balanced by the energy yielded by the fusion reaction itself and the external sources of energy may be turned off. It was shown, that it is not an easy task by British engineer and scientist John David Lawson in his report in 1955 [16], which was published after declassification in 1957 [17]. In his work, he derived three criteria (the *Lawson's criteria*) for temperature, density and confinement time for the deuterium-deuterium (D-D) and D-T reactions as they have the highest cross-sections (probability of interaction) for lowest temperatures of all nuclear fusion reactions (see Figure 6) and also due to the availability of the fuel.

Nowadays, for the D-T reaction the requirement for these parameters is usually written in the following form:

$$n\tau \geq f(T), \tag{8}$$

where $f(T)$ on the right side is a particular function of temperature. The product on the left side has a minimum at $T = 30$ keV, where the ignition $n\tau \geqslant 1.5 \cdot 10^{20}$ m^{-3}s. For a interval of temperatures from 10 keV to 20 keV it is possible to derive another relation called the *triple product*:

$$nT\tau \geq 3 \cdot 10^{21}\ \mathrm{m}^{-3}\mathrm{keVs}. \tag{9}$$

It is important to mention, that the triple product is valid only for the D-T reaction and only for a certain interval of temperatures [19].

For the ICF, Lawson's criteria are identical though they take different form [20], [21].

1.4 Tokamaks

Tokamaks have become a dominant MCF configuration in the thermonuclear fusion research thanks to the acquired results from the experiments conducted on different machines all over the world [22].

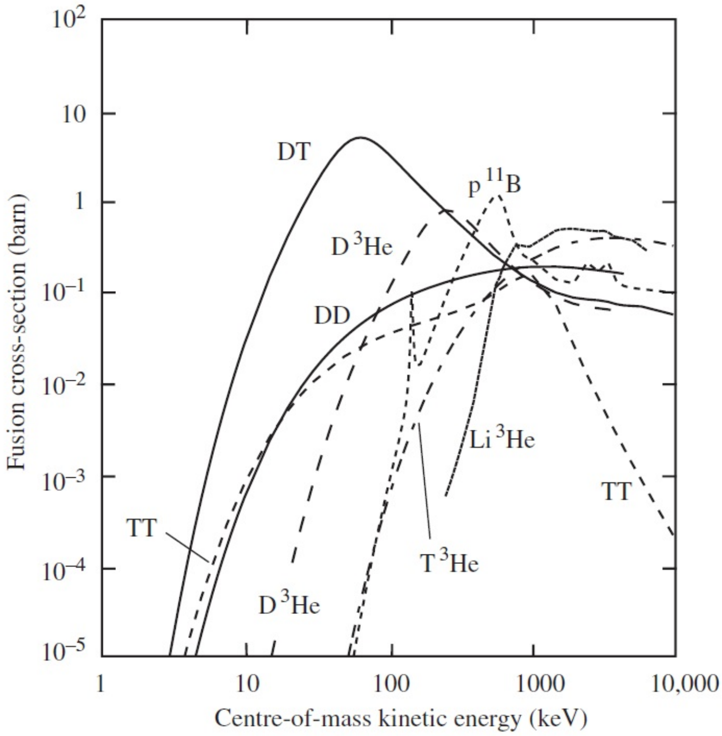

Figure 6: Cross-sections for different fusion reactions with dependency on kinetic energy. The D-T reaction has the highest cross-section. The p -^{11}B reaction produces no neutrons and it is an example of the so-called *advanced fusion* [18].

However, it is also important to mention promising results from the stellarator Wendelstein 7-X [23].

A tokamak is a machine with a set of external coils of a poloidal and toroidal magnetic field to confine hot plasma in the shape of a torus (see Figure 7). The key difference from other MCF configurations is that the tokamak has an electric current flowing through the plasma and high toroidal magnetic field for stabilization purposes.

The core of the tokamak is the transformer core that generates an electric current in the plasma. The plasma acts as the second transformer circuit. The electric current in plasma is generated while there is a current rise in the transformer primary circuit, which makes the tokamak working only in a pulsed regime. As has been already discussed, tokamak has its advantages and disadvantages. For example, an advantage of the electric current flow in plasma is that it acts as a heat source due to the finite resistivity of plasma (Ohmic heating). The current in the plasma generates the toroidal magnetic field. However, it also leads to current-driven instabilities such as kink and sausage instability [4].

The magnetic field in the tokamak can be separated into two regions: high field side (HFS, on the inner side of the torus) and low field side (LFS, on the outer side) magnetic field. Also, there are two components of the magnetic field from the geometric point of view: toroidal field and poloidal field, which is generated by the external coils. The combination of these two fields is a helical magnetic field, which forces trapped plasma particles to go both through HFS and LFS improving stability by suppressing the drifts [4], [25].

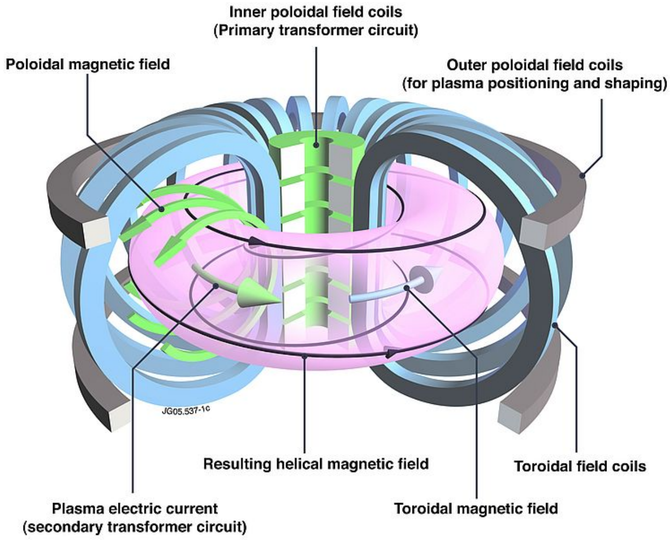

Figure 7: The toroidal shape of plasma in a tokamak. In the center are the inner poloidal coils that generate electric current flow in the plasma. Magnetic field generated by the set of external coils combined with the poloidal magnetic field generated by the plasma current results in a helical magnetic field [24].

Besides the current-driven instabilities, tokamaks have a lot of other different instabilities, due to the plasma in the tokamak being a conductive fluid put in high magnetic fields, that create many of complications in the machine operation [25]. Such instabilities are magnetic islands, MHD instabilities, kinetic instabilities. The last ones are the source of uncontrolled generation of electrons, which could be accelerated to relativistic velocities and even cause damage to the tokamak chamber itself. These electrons are called *runaway electrons* (RE), they will be discussed in more details in the chapter 2.

All the difficulties that tokamaks have met during the past decades had shown, that relatively small machines are not capable of overcoming the problems. This fact has led to an international project called *International Thermonuclear Experimental Reactor* (ITER). This machine will be the largest operating tokamak in the world. Its main goal is to demonstrate the scientific and technological feasibility of thermonuclear fusion energy [26] and to test technologies that will be used in the first nuclear fusion reactor *DEMO* [27]. With the first plasma being planned in the year 2025 [28], the project still has a lot of difficulties to overcome. This has united scientists and engineers all over the world in search for solutions such as choice of appropriate materials for the ITER, that could withstand high neutron and heat fluxes [29], and possible ways to suppress the instabilities [30].

1.5 Thermonuclear fuel

The D-T reaction has the highest cross-section among all possible fusion reactions. Deuterium, or heavy water, is relatively abundant in the Universe: roughly one nucleus of deuterium for 7000 nuclei of hydrogen. Tritium, however, is an unstable isotope of hydrogen with a half-life of 12.3 years and it does not occur naturally in any abundance. Nonetheless, tritium can be bred from isotopes of lithium [31]:

$$^{6}\mathrm{Li} + \mathrm{n} \rightarrow {}^{4}\mathrm{He} + \mathrm{T} + 2.75\,\mathrm{MeV}, \tag{10}$$

$$^7\text{Li} + \text{n} \rightarrow {}^4\text{He} + \text{T} + \text{n} - 2.5\,\text{MeV}, \qquad (11)$$

where first reaction is exothermic with released energy 2.75 MeV, second is endothermic with energy absorbed 2.5 MeV, which makes first reaction favorable for fusion configurations. Lithium is one of the most abundant elements in Earth's crust [32]. Cross-sections for both interactions is shown in Figure 8.

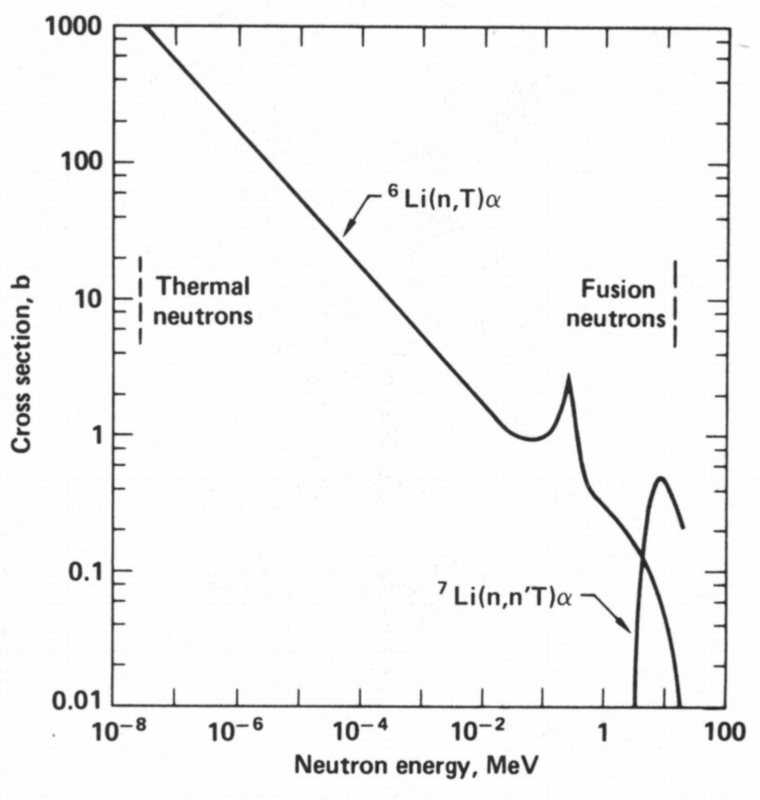

Figure 8: Cross-section of reactions with lithium for tritium production dependent on the incident neutron energy. The reaction with ^{7}Li occurs only for high-energy neutrons. The reaction with ^{6}Li has the highest cross-section at 1000 barns for thermal neutrons [33].

First tokamak tritium breeder will be tested during the ITER campaign in the so-called Test Blanket Modules. These modules will be installed in the first wall of the vacuum chamber facing the hot plasma inside the torus. As can be seen from reaction (10), neutrons are necessary for tritium production. Fortunately, neutrons are produced in the D-T reactions itself (2) and they carry $\frac{4}{5}$ of the total (17.6 MeV) energy produced. Such high energies make neutrons dangerous for the vacuum chamber and different diagnostics in the tokamak configuration, as their impact results in embrittlement and swelling of the material [34].

2 Runaway electrons

Plasma consists of free charge carriers: electrons and ions. In external magnetic fields, these particles undergo helical rotation along the magnetic field lines. Confined particles continue to interact with each other through collisions with a collision frequency ν. These collisions bring a Maxwellian distribution into bulk plasma. However, in the presence of an electric field, some particles can be accelerated. Generally, for particles in an electric field the motion equation may be written in the following form [4]:

$$\frac{\mathrm{d}v}{\mathrm{d}t} = \frac{QE}{m} - \nu(v)v, \tag{12}$$

where Q is the charge of the particle, m is the mass, v is the velocity of the particle, and E is the electric field. Such particles may be either accelerated or slowed down depending on which of the two elements on the right side prevails. It was shown, that collision frequency is dependent on the velocity of the particles as $\frac{1}{v^3}$ [4]. Different regions, where particles are accelerated or decelerated, are shown in Figure 9.

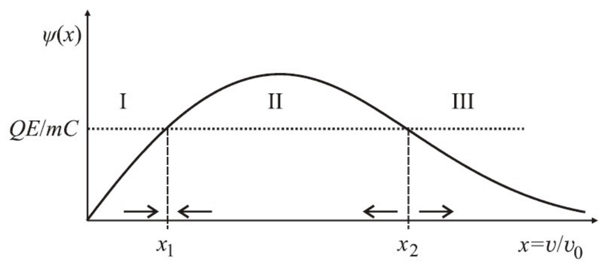

Figure 9: The Chandrasekhar function dependent on ratio of current to initial particle velocity. In the region I particles undergo acceleration by the electric field. In the region II particles are being decelerated via collisions. The region III is the runaway region, where particles undergo acceleration to relativistic velocities. The x_1 point represents the border between the regions I and II which is stable. In the x_2 point the border is unstable and a low amount of external energy may bring particles in a runaway regime [4].

In fusion physics (generally in MCF), one of the crucial points of the ongoing study is runaway electrons (RE). It was recognized as a potential source of damage for tokamak plasma-facing components of the vacuum chamber [35], [36], [37]. For ITER's first plasma being planned just in a couple of years, it is important to develop reliable methods of diagnostics and techniques for their mitigation.

2.1 RE generation

Through the course of study, RE generation was divided into two groups: primary generation by the electric field (Dreicer's mechanism) and the hot tail mechanism and secondary generation due to knock-on collisions between the particles (avalanche mechanism). Nonetheless, these two are not the only possible sources of RE. There are different mechanisms (not only for tokamak plasma but also in astrophysical sources), such as β decay, Compton scattering, magnetic reconnection, cosmic radiation, etc. [38], [39].

2.1.1 Primary generation: Dreicer's mechanism

Mechanism of the primary generation of RE was introduced by American physicist Harry Dreicer in his article in 1959 [40]. The general form for electron velocity was mentioned earlier in this chapter in equation (12). However, to fully understand the mechanism of RE generation, it is necessary to look into details.

To derive a complete motion equation for electrons in plasma, it is necessary to find the collision frequency ν. One can assume a monochromatic beam of tested α particles in a homogeneous isotropic plasma of particles β. With ongoing collisions between the two groups of particles, motion equation for α particles will take the form of Fokker-Planck equation:

$$\frac{\partial f_\alpha}{\partial t} + (\boldsymbol{v}_\alpha \nabla_{\boldsymbol{x}}) f_\alpha + \left(\frac{\boldsymbol{F}_\alpha}{m_\alpha} \cdot \nabla_{\boldsymbol{v}} \right) f_\alpha = S_{\alpha\beta}, \tag{13}$$

where f_α is the distribution function of particles α, $\boldsymbol{v}_\alpha$ and m_α are the velocity and mass of particles α, $\boldsymbol{F}_\alpha = Q_\alpha(\boldsymbol{E}_\alpha + \boldsymbol{v}_\alpha \times \boldsymbol{B}_\alpha)$ is the Lorentz force, where Q_α is the charge of the particles. The term on the right side $S_{\alpha\beta}$ describes collisions between the particles α and β:

$$S_{\alpha\beta} = K_{\alpha\beta} \ln \Lambda_{\alpha\beta} \left[-\frac{m_\alpha + m_\beta}{m_\beta} \nabla_{\boldsymbol{v}} \cdot (f_\alpha \nabla_{\boldsymbol{v}} H_{\alpha\beta}) + \frac{1}{2} (\nabla_{\boldsymbol{v}} \nabla_{\boldsymbol{v}}) : (f_\alpha \nabla_{\boldsymbol{v}} \nabla_{\boldsymbol{v}} G_{\alpha\beta}) \right], \tag{14}$$

where the sign ":" stands for double scalar product. $H_{\alpha\beta}$ and $G_{\alpha\beta}$ are Rosenbluth potentials for friction and diffusion respectively:

$$H_{\alpha\beta} \equiv \int \frac{1}{g} f_\beta \mathrm{d}^3 \boldsymbol{v}_\beta,\ G_{\alpha\beta} \equiv \int g f_\beta \mathrm{d}^3 \boldsymbol{v}_\beta,\ g \equiv |\boldsymbol{v}_\alpha - \boldsymbol{v}_\beta|, \tag{15}$$

and $\ln \Lambda_{\alpha\beta}$ is the Coulomb logarithm (6). The constant $K_{\alpha\beta}$ is defined:

$$K_{\alpha\beta} \equiv 4\pi \left(\frac{Q_\alpha Q_\beta}{4\pi\varepsilon_0 m_\alpha} \right)^2. \tag{16}$$

This is a general form of Fokker-Planck equation that is used to describe kinetic instabilities and RE.

The probability distribution of the beam of α particles is given by the Dirac distribution function:

$$f_\alpha = n_\alpha \delta(\boldsymbol{v}_\alpha - \boldsymbol{v}(t)). \tag{17}$$

The probability distribution of plasma particles is given by the Maxwellian distribution:

$$f_\beta = n_\beta \left(\frac{m_\beta}{2\pi \mathrm{k_B} T_\beta} \right)^{\frac{3}{2}} \exp\left[-\frac{m_\beta v_\beta^2}{2\mathrm{k_B} T_\beta} \right], \tag{18}$$

where n_α and n_β are densities of the particles, $\mathrm{k_B}$ is the Boltzmann constant and T_β is the temperature of particles β. A monochromatic beam of particles is equivalent to one particle, so particles α cannot undergo diffusion. That means, that only frictional potential $H_{\alpha\beta}$ must be taken into consideration.

Using the expressions above, the Chandrasekhar function is defined as:

$$\psi(x) \equiv \frac{2}{\sqrt{\pi} x^2} \int_o^x \xi^2 \exp[-\xi^2] \mathrm{d}\xi \tag{19}$$

and finding the first moment of the Fokker-Planck equation (13), one can derive:

$$\frac{\partial \boldsymbol{v}}{\partial t} = \frac{\mathrm{e}E}{m_\mathrm{e}} - 2n_\beta K_{\alpha\beta} \ln \Lambda_{\alpha\beta} \frac{m_\alpha + m_\beta}{m_\beta} v_{0\beta}^{-2} \psi\left(\frac{v}{v_{0\beta}}\right) \frac{\boldsymbol{v}}{v}, \tag{20}$$

which is the motion equation for electrons in plasma with an external electric field, where $v_{0\beta}$ stands for initial velocities of β particles before the collisions, e is the charge of an electron and m_e is the mass of an electron. The particles in tokamak plasma that undergo collisions with electron beam are both electrons and ions. The drag force, which is a result of collisions between the particles, can be written in the next form [41]:

$$F_\mathrm{d} = \frac{n_\mathrm{e} \mathrm{e}^4 \ln \Lambda}{4\pi\varepsilon_0 m_\mathrm{e}} \left[\frac{Z_\mathrm{eff}}{v_{0\mathrm{i}}^2} \psi\left(\frac{v}{v_{0\mathrm{i}}}\right) + \frac{2}{v_{0\mathrm{e}}^2} \psi\left(\frac{v}{v_{0\mathrm{e}}}\right)\right], \tag{21}$$

where $Z_\mathrm{eff} = \frac{\sum_i Z_i^2 n_i}{n_\mathrm{e}}$ is the effective ion charge.

The motion equation may also be written using so-called *Dreicer's field* E_D, which was derived by Harry Dreicer in his article [40] as critical field:

$$\frac{\partial v}{\partial t} = \frac{\mathrm{e}E}{m_\mathrm{e}} - \frac{2\mathrm{e}}{m_\mathrm{e}} E_\mathrm{D} \psi\left(\frac{v}{v_{0\beta}}\right), \; E_\mathrm{D} = \frac{n_\mathrm{e} \mathrm{e}^3}{4\pi\varepsilon_0^2 \mathrm{k_B} T_\mathrm{e}} \ln \Lambda \tag{22}$$

The Dreicer's field E_D is called "critical", because when the electric field in plasma E increases above the Dreicer's field, all electrons enter runaway regime and are constantly accelerated to relativistic velocities.

However, if relativistic effects on RE generation are taken into consideration, one could derive another "critical" field, called the *Connor-Hastie field* $E_\mathrm{CH} = \frac{n\mathrm{e}^3}{4\pi\varepsilon_0^2 m_\mathrm{e} c^2} \ln \Lambda$. In the electric field $< E_\mathrm{CH}$ no runaway electrons can be generated [38], [42]. Both Dreicer's and Connor-Hastie's fields are shown in Figure 10.

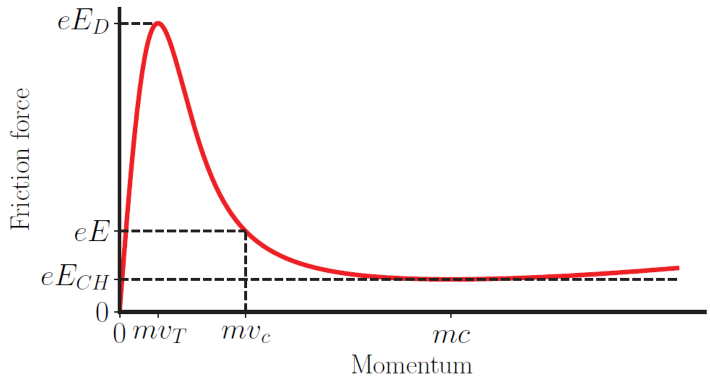

Figure 10: Dependency of the friction force ψ on particle's momentum. For electric field above E_D all particles enter runaway regime, for field above E_CH particles with momentum higher than mv_c enter runaway regime [38].

The Dreicer's mechanism of RE generation serves as the seed of RE generator, for these electrons are multiplied in numbers further via other mechanisms. This primary mechanism takes place in small and medium-sized tokamaks with lower plasma densities. In larger tokamaks, RE seed could be generated via the so-called *hot tail mechanism* [43].

2.1.2 Primary generation: Hot tail mechanism

The hot tail mechanism is the main source of RE in larger tokamaks. This mechanism is connected with a phenomenon in tokamak physics called *disruption*. Generally, "disruption" is a term that describes a series of events that lead to a loss of confinement and terminates the discharge. The main event that characterizes disruptions is a thermal quench (TQ), which is a sudden fall of plasma temperature in time [44]. Thermal quenches (and disruptions generally) can be initiated by impurities, which cools down the plasma via radiation losses.

Bulk plasma has a Maxwellian distribution (Figure 11). Impurities put into the plasma add cooler electrons via ionization while cooling the plasma by excitation/deexcitation process. Electrons from the bulk plasma interact with cooler particles via collisions. However, for hotter electrons this process takes more time because the collision frequency is lower for higher energies. This leaves the fastest electrons from the initial Maxwellian distribution no particles to interact with and, similar to Dreicer's mechanism, for these electrons acceleration by the electric field prevails. A more detailed description of the hot tail mechanism can be found, e.g., in [45].

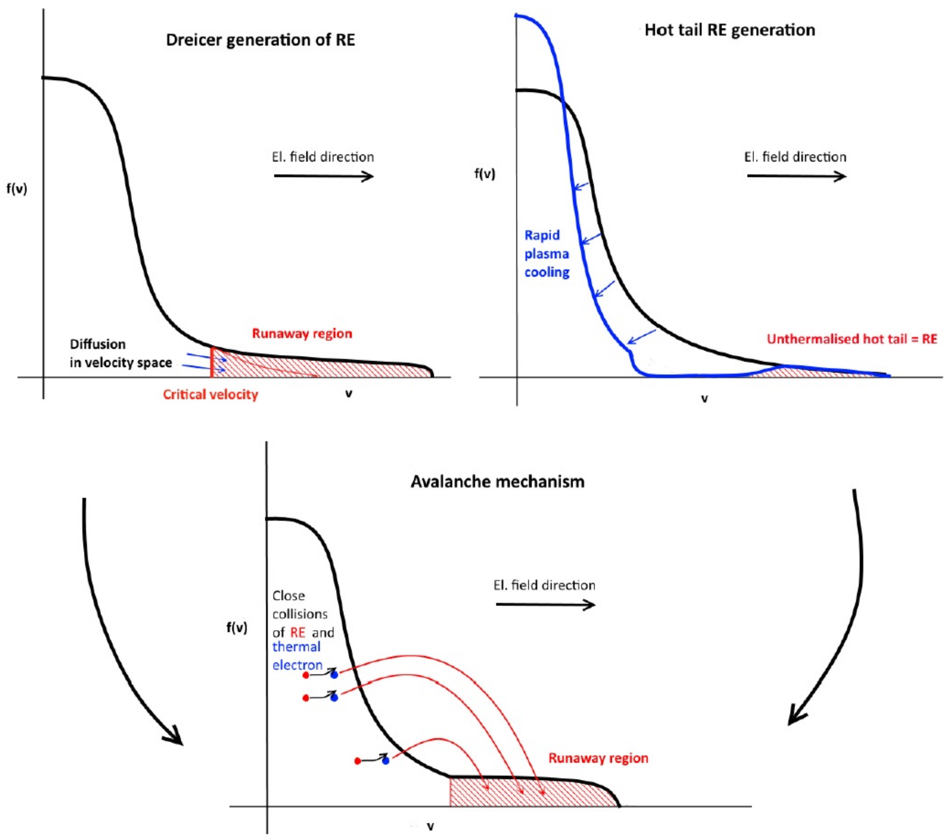

Figure 11: Schematic illustration of the primary mechanisms of RE generation and the multiplication of REs via the avalanche mechanism [41].

2.1.3 Secondary generation

Through the course of RE studies, it was proved, that in large tokamaks, primary mechanisms are not sufficiently strong to produce abundant runaway electrons [38]. The large growth of the number of runaway electrons is caused by another mechanism - the *avalanche* mechanism of RE generation. This source of REs is considered as secondary because it demands that some REs have been already generated and these particles can undergo rapid multiplication. The term "avalanche" stands for a series of so-called *knock-on* collisions between the REs and thermal electrons in the bulk plasma. During these collisions, REs transfer their momentum to thermal electrons, giving them sufficient energy to enter runaway region, while sustaining in the runaway regime itself. Newly pushed thermal electrons are then undergoing acceleration by the electric field, same as primary REs, and further on may bring more thermal electrons to the RE region. An analytical description together with testing via Monte Carlo modeling was provided by Rosenbluth and Putvinski in their article in 1997 [46]. The article also states, that while primarily generated REs may achieve energies up to 100 MeV, REs generated via the avalanche mechanism have energies up to 10-20 MeV. Similar to the hot tail mechanism, the avalanche mechanism occur during the thermal quenches in disruptions. The avalanche mechanism of RE generation is shown schematically in Figure 11.

2.2 RE diagnostics

REs are considered a potential danger for large tokamaks, especially for ITER. This brings up a question of possible techniques for diagnostics of REs and mitigation of either source of RE generation (i.e. prevention of disruptions) or their impact on plasma-facing components. The following text will describe ways of how RE can be detected. Physical processes, on which these diagnostics rely, will be described in the next chapter.

REs cover a vast spectrum of energies from a few keV to tens of MeV. However, there is no such diagnostic method, that can detect and measure this wide range of energies. Through the course of RE studies, many different solutions were developed. The majority of REs diagnostics rely on the measurement of different emissions from the plasma caused by interactions of REs either with particles of the bulk plasma (generally ions) or with the plasma-facing material (first wall or divertor).

One of the most used diagnostics is the detection of photons produced via so-called *bremsstrahlung* emission (section 3.1). These photons are usually divided into two groups: with energies from a few eV to approximately 5 keV (soft X-rays, SXR), and with energies from 5 keV to approximately 50 keV (hard X-rays, HXR). Above that are gamma-rays with energies > 50 keV [47]. For both groups, different diagnostics are used. While SXR can be detected by semiconductor detectors, for HXR with higher energies scintillators are used. Semiconductor detectors will be discussed later in this work in chapter 4.

Scintillators detect X-rays produced during an impact of REs onto the wall material. The photons produced via bremsstrahlung are transformed into visible light in luminescent materials. Generally, scintillators vary in the density of the material, which influence the probability of gamma-ray interaction, in the brightness of the material, which describes the amount of visible light produced per X-ray absorbed, and in the measurement time (how fast the signal can be generated). In tokamak diagnostics, the most common are NaI(Tl), BGO, and LaBr3(Ce) scintillating materials that have different properties (i.e. signal level, decay time). The conversion into visible light is possible due to the photoelectric effect, Compton scattering and production of electron-positron pairs (section 3.2), which is possible only at relativistic energies. The light is further transformed into an electric signal via the photoelectric effect in a photocathode. To make the signal measurable, electrons are multiplied in numbers during a series of collisions on dynodes. The schematic illustration of the detector can be seen in Figure 12.

Another way to detect REs is measuring of electron cyclotron emission (ECE). Every particle with a charge put in an external electromagnetic field undergoes a rotation with frequency given by (3). However, for an electron to emit or to absorb an electromagnetic wave with a wave vector $\boldsymbol{k}$, a certain condition for the particle's frequency must be satisfied:

$$\omega = n\frac{\omega_{\text{ce}}(\boldsymbol{B})}{\gamma} + k_{||}v_{||}, \tag{23}$$

where n stands for n-th harmonic contribution and index $||$ stands for the component parallel to the magnetic field $\boldsymbol{B}$ [48]. The γ factor represents relativistic effects. REs generated during disruptions contribute to the general ECE signals intensifying them. By measuring the power of those signals one can compute REs temperature [49].

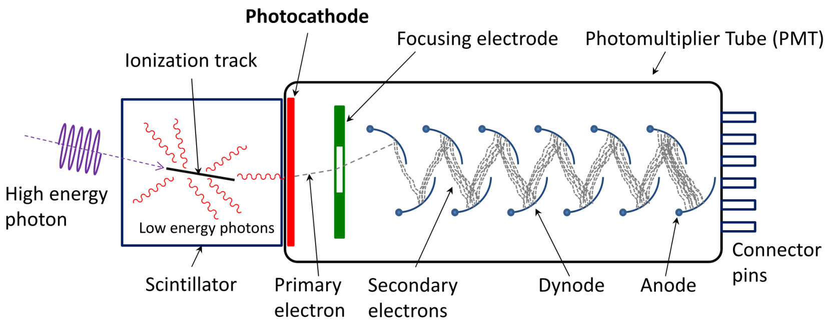

Figure 12: A schematic illustration of a scintillator detector. Incident photon with high energy produces photons in visible range in the scintillating material. The primary electric signal is generated on the photocathode via photoelectric effect. The signal is further intensified in a series of collisions on the dynodes [50].

For ECE measurements, radiometers and interferometers are used. The first one acts as a passive diagnostic measuring power level of ECE and provides fast measurements with frequencies higher than 1 MHz and rough spectral resolution ($\sim$ 1 GHz). The second one acts as active diagnostic emerging light into the plasma and afterwords measuring refracted radiation. Interferometers provide slow measurements with frequencies lower than 100 Hz, but with higher spectral resolution ($<$ 1 GHz) [38].

Diagnostics of boundary REs can be conducted via probes. Some probes have a similar purpose as scintillator detectors measuring emission produced by REs in the outer regions of the plasma. However, for the probes being emerged into the vacuum vessel, the potential damage of the diagnostic from the hot plasma and neutron flows complicates the measurement. It is necessary to shield the probes using the same materials as for the first wall, i.e., tungsten. Another kind of probes measures the so-called *Cherenkov emission*. Both types of probes have a faster time response than the scintillator: $<$ 1 ns for the probes compared with $>$ 100 ns for the scintillators [38]. A calorimeter probe for REs measurement was designed and tested at the TEXTOR tokamak. This probe acts as a target for the RE beam, which hits the probe, depositing energy in the material and consequently heating it. The measurement provides information about RE energy during disruptions [51].

Infra-red (IR) thermography can be used to study heat loads of RE beams onto the first wall material. Unlike probes, IR imaging is a remote diagnostic and covers larger areas of the vacuum chamber. While IR provides with a possibility of monitoring RE impacts on the first wall, quantitative analysis is rather challenging [38].

Apart from radiation emission generated by REs, measurement of neutron emission is also possible for the RE diagnostics. Generally, neutrons are generated in D-D and D-T fusion reactions. However, when REs are generated, neutrons can be produced via photo-neutron nuclear reactions in the first wall material. Photo-neutrons can be measured with many different detectors, from scintillators to semiconductor detectors. Apart from the usual construction of these detectors, plastic filters are used to transfer neutrons to protons via (n,p) reactions. Protons are charged particles and their detection is not as complicated as neutron detection. Photo-neutron signals act as a notification that there was an impact of REs with the first wall [38].

2.3 RE mitigation

Disruptions are unfavorable in tokamak operation because they shorten the machine's lifetime. As has been already mentioned, REs generated during disruptions are detrimental to the first wall of the vacuum chamber as they can damage the material. Besides that, disruptions lead to other dangerous processes such as high heat flux onto the first wall material and large forces in the tokamak's structures from the so-called *halo currents* [52]. This raises a question of possible disruption mitigation strategies, that have lead to developing of the *disruption mitigation system* (DMS). DMS relies on the injection of material into the plasma to suppress RE generation and dissipate the energy stored in RE beams. The system follows two strategies: massive gas injection (MGI) and shattered pellet injection (SPI) [38]. Experiments on DIII-D tokamak have shown, that SPI technique has deeper penetration of the injected material into the plasma than MGI [53]. However, MGI systems have been successfully implemented and tested at tokamak JET with ITER-like wall [54]. Both systems are being prepared for the ITER's DMS.

Gas or pellet injection can be activated in different moments of disruption development: pre-TQ (thermal quench), post-TQ and during RE generation. Disruption mitigation systems have several goals to accomplish. One of them is to boost losses via radiation to reduce conductive losses of energy stored in plasma. During TQs, high heat fluxes arise, bringing a vast amount of thermal energy onto the plasma-facing components. This could lead to material melting. However, this is not a simple task, as energy dissipation has to be fast enough to mitigate the damage and it has to be homogeneous through all the targeted area. Another mission of the DMS is to prevent RE generation. This could be achieved via densification by injection of the material (i.e. deuterium) into the bulk plasma, which for the electron component would balance the acceleration by the electric field by collisions. The development of disruption mitigation systems goes along with the development of diagnostic systems and models of the tokamak operation [38].

3 Interactions of radiation with matter relevant for RE detection

This chapter summarizes some of the most important processes of the interaction between radiation and matter relevant for the detection of REs. Generation of bremsstrahlung is the dominating process of REs energy loss. Detection of REs relies on the detection of photons that are produced during interaction of REs either with plasma particles or with the inner wall of the tokamak. However, photons may interact with matter in different ways depending on their energy and the material. Another way to follow RE beams is to detect neutrons that a produced during impacts of the REs onto the tokamak's first wall.

3.1 Bremsstrahlung

Bremsstrahlung is electromagnetic radiation produced by a charged particle during acceleration or deceleration in the electric field of another charged particle. Schematically this process is shown in Figure 13. In plasma, electrons undergo acceleration by the Coulomb interaction with ions more often than deceleration on other electrons. Also, bremsstrahlung can be produced during collisions of high energetic RE on the inner wall of tokamak.

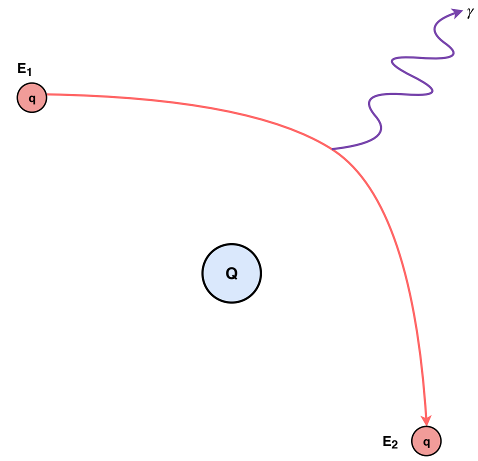

Figure 13: Bremsstrahlung emission: photon of energy $h\nu = E_2 - E_1$ is produced by the decelerated particle with charge q in the electric field generated by the particle with charge Q.

The power loss of RE beam via bremsstrahlung produced during acceleration by ions is given in the following formula [25]:

$$P_{\mathrm{br}} = 5.35 \times 10^{-37} Z^2 n_{\mathrm{e}} n_{\mathrm{z}} T_{\mathrm{e}}^{\frac{1}{2}}, \tag{24}$$

where Z is the ion atomic number, n_{e} is electron density, n_{z} is the ion density and T_{e} is electron temperature. The equation shows, that power loss via bremsstrahlung has a quadratic dependence on ion charge. Therefore, if impurities with high atomic number Z are present in plasma, bremsstrahlung becomes enhanced. Measurements of the bremsstrahlung emission produced by REs give information about their temperature.

The spectrum of bremsstrahlung photons is continuous, photon's energy may extend as high as electron energy. With the use of specific filters, it is possible to remove photons with lower energies thus shaping their spectrum [55].

3.2 Photons

Photons generated via bremsstrahlung emission from RE, that interact either with bulk plasma or with the tokamak's wall material, cover a vast range of energies from a few keV to tens of MeV. Energetic photons are usually measured by scintillator detectors. There are several different mechanisms of radiation-matter interaction at play in scintillator detectors which will be covered in this section.

Generally, X-rays are converted into visible light in scintillators via three mechanisms: photoelectric effect, Compton scattering, and pair production depending on the incident photon's energy and the interacting atoms of the material [38], [56]. These mechanisms of photon-matter interaction are shown in Figure 14.

The photoelectric effect is the emission of electrons during an impact of radiation onto the material. Generally, electrons in atoms are bound, populating certain orbits given by their energy. Each orbit has a so-called *ionizing energy* U_{ion}, which is the energy needed for the electron to overcome attractive strong nuclear forces and become free. If the incident photons have energy $E = h\nu > U_{\text{ion}}$, then they are absorbed by the atom. Part of the energy is spent on ionization of the atom, setting an electron free. The rest of the photon's energy is transformed into the kinetic energy of the electron. If the photon's energy is not enough for an electron to become free, during an impact it is still absorbed; however, this leads to the excitation of the atom, an electron is pushed to the next orbit further from the nucleus. During deexcitation, the electron loses some energy and returns to a lower orbit, radiating a photon during the process. The photoelectric effect occurs when photons of energies from a few eV to a few keV interact with the material.

During Compton scattering, a photon is scattered by a charged particle. Usually, Compton scattering occurs on electrons that are loosely bound on outer orbits. For the reaction to occur, photons must have certain energy $h\nu_{\text{c}}$. For such photons, these electrons can be considered as stationary. During the interaction, photon passes some of its energy to the electron and scatters at some angle with reduced energy $h\nu'$. After the interaction electron becomes so-called *Compton electron*, which is ejected from the atom with kinetic energy $E_{\text{kin}} = h\nu_{\text{c}} - h\nu'$. Compton scattering occurs when photons have energies between a few keV to a few MeV, when pair production mechanism becomes dominant.

When a photon with energy above 1.022 MeV (which is the energy needed to produce an electron-positron pair) passes close to a nucleus, it may interact with the nucleus, producing a pair of an electron and positron. Their kinetic energy combined is given by $E_{\text{kin}} = h\nu - 1.022$ MeV. The electron and positron are then flying off, interacting with the surrounding material, losing their energy. Positron loses its energy with a much faster rate because it is an anti-particle to the electron and interacting with a free electron it annihilates producing two photons with energies of 0.511 MeV [56].

The dominant interaction mechanisms for different photon energy and different materials (different values of Z) are shown in Figure 15. All mechanisms of the photon-matter interaction for ^{14}Si are shown in Figure 16.

3.3 Photo-neutrons

Neutrons are generally produced during D-D and D-T fusion reactions. However, if REs are present in a tokamak, photo-neutrons can be generated during an impact of REs with the tokamak's wall. The interaction of REs with the material of the wall results in the generation of photons, which are emitted

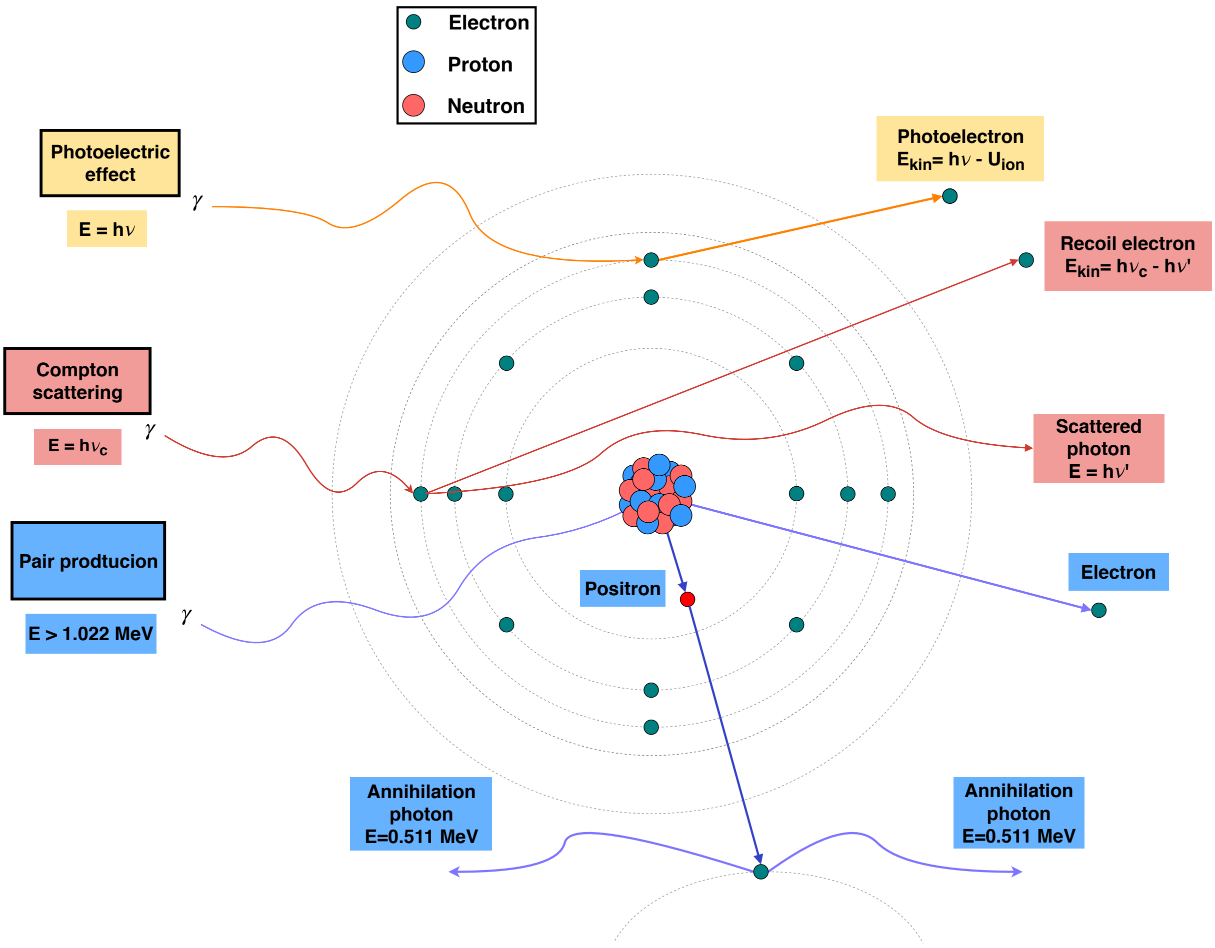

Figure 14: The photoelectric effect (in yellow), Compton scattering (in red) and the pair-production mechanism (in blue) in an atom of silicon.

in different directions towards the wall material. These photons continue to interact with electrons and nuclei. If a photon has sufficient energy, it may interact with a nucleus. The interaction takes the next form:

$$ {}^{i}_{j}X + \gamma \rightarrow {}^{i-1}_{j}Y + \mathrm{n}, \tag{25} $$

where X is the initial nucleus with atomic number $A = i$ and j protons, γ is the incident photon, Y is the resulting nucleus with atomic number $A = i - 1$. The binding energy of the nucleus plays the role of a threshold energy for the photo-nuclear production [59].

Photo-neutrons continue to travel through the material. However, their interaction with the surrounding particles greatly differs from the interaction of charged particles. In general, neutrons have no charge, so they do not interact with charged particles via Coulomb forces, which makes neutron measurement difficult. The only interaction that a neutron can undergo is a collision with a nucleus of the absorbing

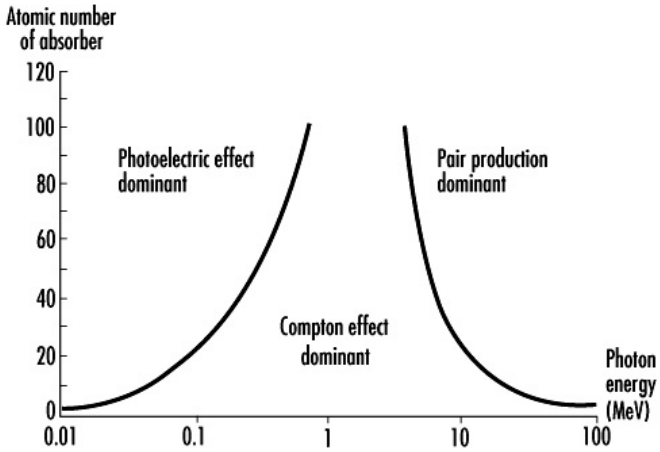

Figure 15: Three main mechanisms of the photon-matter interaction depending on the Z number of the target atoms and the photon's energy. Solid lines show the values of Z and $h\nu$ for which the two neighboring effects are equal [57].

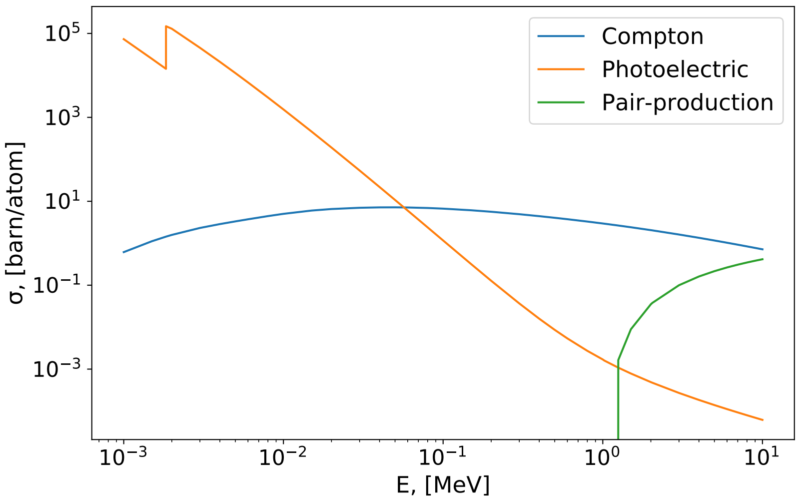

Figure 16: Mechanisms of the photon-matter interaction for ^{14}Si depending on the photon's energy. Data acquired from [58].

material. Interactions between photo-neutrons and nuclei can be divided into two groups depending on the initial energy of neutrons.

For slow neutrons with low energies, elastic scattering and neutron-induced nuclear reactions prevail. Elastic collisions bring such neutrons to the thermal equilibrium with their surroundings, as they transfer their energy to nuclei. More important are nuclear reactions which can be initiated by incident neutrons. Such nuclear reactions must have a positive value of the reaction energy Q. Also, nuclear reactions can act as a source of secondary radiation. For most materials, neutron capture, or (n,γ), is the most probable. However, for neutron detection purposes it is not favorable, as photons are also difficult to detect. For more precise detection, reactions such as (n,α) or (n,p) should be used, because the products are charged particles that can be easily detected. For these, different plastic filters can be used.

Fast neutrons are much more difficult to detect because the probability of their interaction with a nucleus is lower. However, their energy can be lowered via a series of scattering interactions. During scattering, fast neutrons slow down, transferring their energy to the recoil nuclei, that act as secondary radiation. To lower neutron's energy, moderators are used, the hydrogen being most sufficient. If the neutron has sufficiently high energy, inelastic scattering may occur. The targeted nucleus becomes excited, followed by a photon emission. This plays an important role in shielding of high-energy neutrons. However, gamma photons are unfavorable for the neutron diagnostics as they contribute to the neutron signal and by that complicate the data analysis [55].

4 Semiconductor detectors

4.1 Semiconductor materials

All solid materials depending on their electrical conductivity can be divided into three groups: conductors, insulators and semiconductors. Properties of these materials are dictated by their periodic lattice structure, which establishes two energy bands that electrons are allowed to occupy. The first one is the *valence band* that corresponds to the electrons in outer shells of atoms and which occupy specific sites in the crystalline lattice. The second one is the *conduction band*, which represents free electrons that migrate through the crystal. The bands are divided by the *bandgap* where no electrons are allowed. The width of the bandgap is given by bandgap energy E_g, which is the energy that electrons have to acquire to transfer from the valence band to the conduction band. Conductors have many free electrons because the two bands are either very close to each other or they even overlap. A small amount of external energy provides electrons with sufficient energy to go into the conduction band. This makes conductors to easily allow the flow of electric current. On the other hand, insulators have almost no free electrons because of the wide bandgap with $E_\mathrm{g} > 5$ eV. Electrical conductivity of the semiconductors lies in between the conductors and insulators. Bandgap energy for the semiconductors is ≈ 1 eV [55]. Band structures for all the three groups of materials is shown in Figure 17.

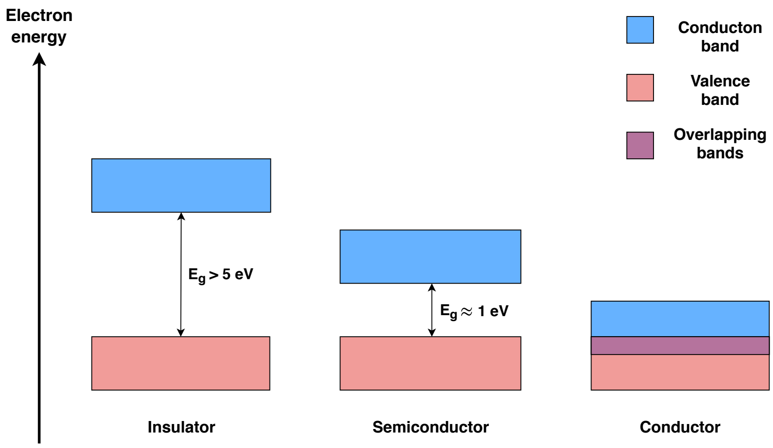

Figure 17: The conduction and the valence band in insulators, semiconductors, and conductors. E_g is the bandgap energy. While there is a gap between the bands in insulators and semiconductors, the bands in conductors overlap.

Generally, all electrons in the crystals share some thermal energy. It is possible for an electron trapped in the valence band to gain sufficient energy to transfer into the conduction band. During such an excitation process not only an electron is transferred to the conduction band, but also a vacancy (a hole) is created in the valence band. The pair of such electron and hole is called *electron-hole pair*. If an external electric field is applied, the electron will move in one direction and the hole will move in the opposite. The electrons from the valence band may fill the hole creating a new one, which represents a new position of the initial hole. The motion of such electron-hole pairs contributes to the conductivity of the material. With no electric field applied, electrons and holes will undergo diffusion. The probability for the generation of an electron-hole pair depending on the temperature is [55]:

$$p(T) \approx T^{\frac{3}{2}} \exp\left[-\frac{E_\mathrm{g}}{2k_\mathrm{B}T}\right]. \tag{26}$$

If no electric field, that separates the electrons from the holes, is applied, they will recombine by returning the electron to the valence band. The concentration of the electron-hole pairs strongly depends on the temperature and will decrease if the material is cooled.

Generally, in the presence of an external electric field, the motion of the electron-hole pairs is a combination of their thermal velocity and a net drift velocity parallel to the electric field. At low values of the electric field, the drift velocity is proportional to the applied field and for high values the velocity reaches a saturation. Usually, semiconductor detectors are operated with electric field of sufficient values to reach the saturation velocities in order of 10^7 cm/s. Typical dimensions over which the charge carriers are collected are of the order of 0.1 cm. The time of the collection is then under 10 ns [55].

There are many known materials with semiconductor properties. Most common are silicon and germanium due to cheap production technology and their suitable characteristics for radiation detectors [60]. All semiconductor materials differ in the bandgap energy, electron a hole mobility, etc. Wider bandgap allows some semiconductor materials to work in higher temperatures with low thermal noise. Electron and hole mobility influence the rate of operation, i.e. the signal collection time. Pure semiconductors are called *intrinsic* semiconductors. Their key characteristic is that electron-hole pairs may be generated only through thermal excitation or due to ionizing radiation. However, all materials have impurities that influence their properties. It is also possible to dope semiconductor materials with impurities to achieve some favorable parameters. Through doping, semiconductors can gain either more free electrons in the conduction band, or more holes in the valence band than intrinsic materials. Such semiconductors are called n-type or p-type, respectively.

4.1.1 n-type semiconductors

Semiconductors of the n-type may be created via doping the intrinsic material, i.e. silicon, which is tetravalent, with atoms of pentavalent materials, i.e. with phosphorus. Atoms of the latter will substitute atoms of silicon in the crystalline lattice with 4 electrons creating a covalent bond a one electron left. The crystalline structure of silicon doped with phosphorus is shown in Figure 18. This electron is loosely bound to the impurity atom and a small amount of energy will transfer it to the conduction band. Impurities of this type are called *donor* impurities, as they bring more free electrons into the material. The electrons that impurities bring into the material have lower energy gap than the bulk electrons. This allows electrons to enter the region, which is forbidden for electrons in intrinsic semiconductors, between the conduction and the valence band. The electrical conductivity of donor-doped semiconductor is larger than that of the intrinsic material due to the balance between electrons and holes being shifted to the electron part. As electrons dominate in the electrical conductivity, they are called *majority carriers*, which leaves holes as *minority carriers* [55]. The energy band structure is schematically shown in Figure 19. Such semiconductors are called n-type because majority of the carriers have negative charge.

4.1.2 p-type semiconductors

Doping silicon with a trivalent material, i.e., boron will create a semiconductor of the p-type. Impurity atom will substitute a silicon atom in the crystalline lattice, filling only three covalent bonds with one left unsaturated. This creates a vacancy which represents a hole in the valence band. In such semiconductors there is a higher probability of recombination of electron in the conduction band with a hole in the valence band. Electron that will fill this vacancy saturates the fourth covalent bond, however, it is loosely bound as one of the two participating atoms is a trivalent impurity. The crystalline structure of silicon doped with boron is shown in Figure 20. The energy required for the loosely bound electron to

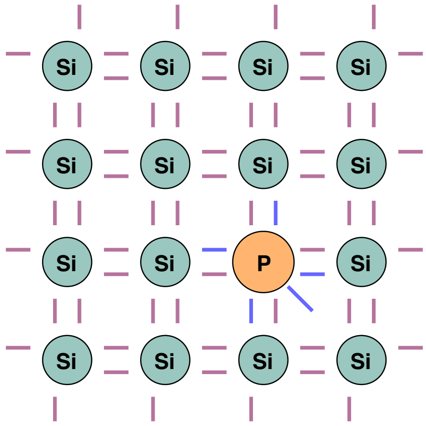

Figure 18: Crystalline lattice structure in silicon doped with phosphorus. Each dash represents an electron, the impurity atom has one electron that is loosely bound.

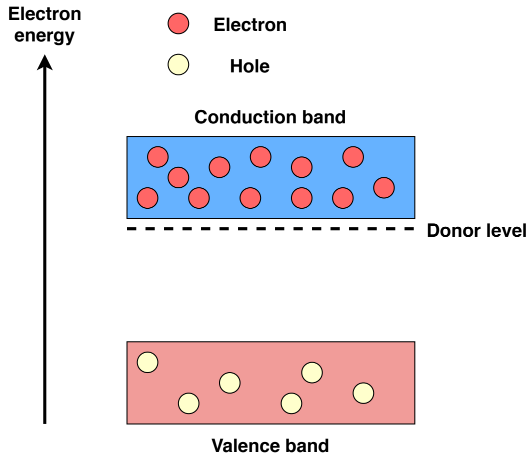

Figure 19: Energy band structure in the n-type semiconductors. Electrons in the conduction band are the majority carriers. Donor level represents lower energy level for impurities' electron.

become free and enter the conduction band is slightly lower than for the bulk electrons from the Si-Si bonds. Such impurities are called *acceptor* impurities as they are willing to accept an electron from the bulk material. In a boron-doped silicon there are more holes than free electrons, the balance is shifted and holes dominate in the electrical conductivity. In this case holes are majority carriers [55]. The energy band structure is schematically shown in Figure 21. Semiconductors with fewer free electrons than holes in the valence band are called p-type because majority of carriers have positive charge.

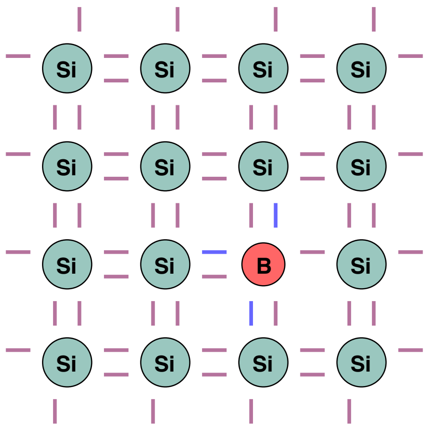

Figure 20: Crystalline lattice structure in silicon doped with boron. Each dash represents an electron, the impurity atom has a vacancy representing a hole.

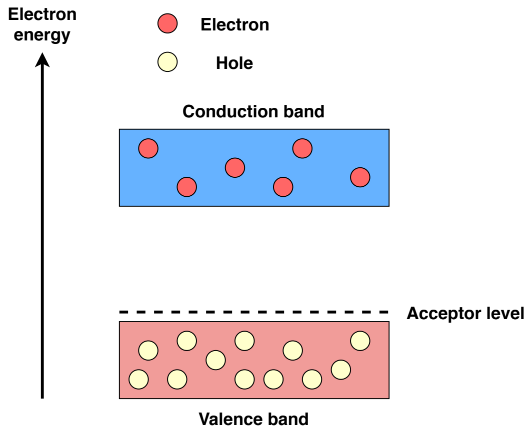

Figure 21: Energy band structure in the p-type semiconductors. Holes in the valence band are the majority carriers. Acceptor level represents higher energy level for impurities' holes.

4.2 Semiconductor detectors

The electron-hole pairs can be created either via thermal excitation or as a result of ionizing radiation. The latter makes semiconductor materials acceptable as the ionizing radiation detectors. A charged particle that passes through the semiconductor will lose its energy via interaction with electrons and ions in the material. This will make electrons leave their occupied sites in the crystalline lattice and move freely in the crystal. The vacancy left by the electron is then represents the hole. The electron-hole pair is created *directly* by the ionizing radiation. High-energy electrons created by the radiation continue to interact with other bound electrons, giving them some of their energy. If the transferred energy is sufficient for the generation on and electron-hole pair, in this case the pair is created *indirectly*. Regardless of the mechanism, equal amount of electrons and holes is created independent on the type of the semiconductor. For an electron to leave its place in the crystalline lattice, radiation must pass sufficient energy called the *ionization energy* ε [55]. The rest of the depleted energy is transferred into the kinetic energy of the electron.

One of the advantages that semiconductor materials have, is the low ionization energy: for silicon ε = 3.76 eV and for germanium ε = 2.96 eV at the temperature of 77 K. In comparison, for the gas-filled detectors the ionization energy is about 30 eV [55]. Therefore, for the equal amount of energy lost by the charged particle in both types of the detectors, in semiconductors there are more charge carriers created than in gas-filled detectors.

The semiconductor detectors usually operate either cooled (i.e. germanium detectors cooled to the temperature of liquid nitrogen, 77 K) or in a depleted state. A combination of the p-type and n-type materials is called *semiconductor p-n junction*. Such junctions are created via alternative doping process, when half of the material is donor-doped and the other half is acceptor-doped. As the n-type semiconductors have more negative electrons and the p-type have more positive holes, in a combination a charge diffusion will occur: the electrons from the conduction band of the n-type will be attracted by the holes in the valence band of the p-type semiconductor. Upon meeting, electrons and holes will recombine, bonding free electrons into the crystalline lattice. Both in the n-type and p-type semiconductors there is an imbalance in the electron and hole number. However, the charge is maintained neutral due to impurity ions in the material. The diffusion of the electrons from the n-type leaves immobile positive ions and after the recombination a negative charge will appear in the p-type semiconductor. This process generates electric field that will stop further charge diffusion. This will create a region called the *depletion region* between the n-type side and the p-type side of the junction. The potential difference created by the charge distribution is called *contact potential*. Its value in the equilibrium state is as high, as the bandgap energy in the semiconductor material itself. If a charged particle will enter the depletion region and create electron-hole pairs, the latter will be separated by the electric field: electrons will be pushed into the n-type side and holes into the p-type side. This makes the semiconductor junction favorable for the particle and radiation detection purposes. A p-n semiconductor junction with no bias voltage applied is shown in Figure 22. Width of the depletion region is dependent on the bias voltage applied to the p-n junction and the concentration of acceptor or donor atoms (see Figure 23).

An external electric field will make charge carriers in the semiconductor material go in the opposite direction towards electrodes. By applying an external field to the p-n junction, a p-n diode will be created. If the field is applied in such a way, that the positive voltage is on the p-type side, the resulting potential will attract majority charge carriers from the both sides. This will lower the potential difference seen by an electron resulting in the lower contact potential. This is known as the *forward biasing*. If the external electric field is applied in the opposite way, that the positive voltage is present on the n-type side, the resulting potential will attract minority carriers from the sides. This is known as the *reverse biasing*.

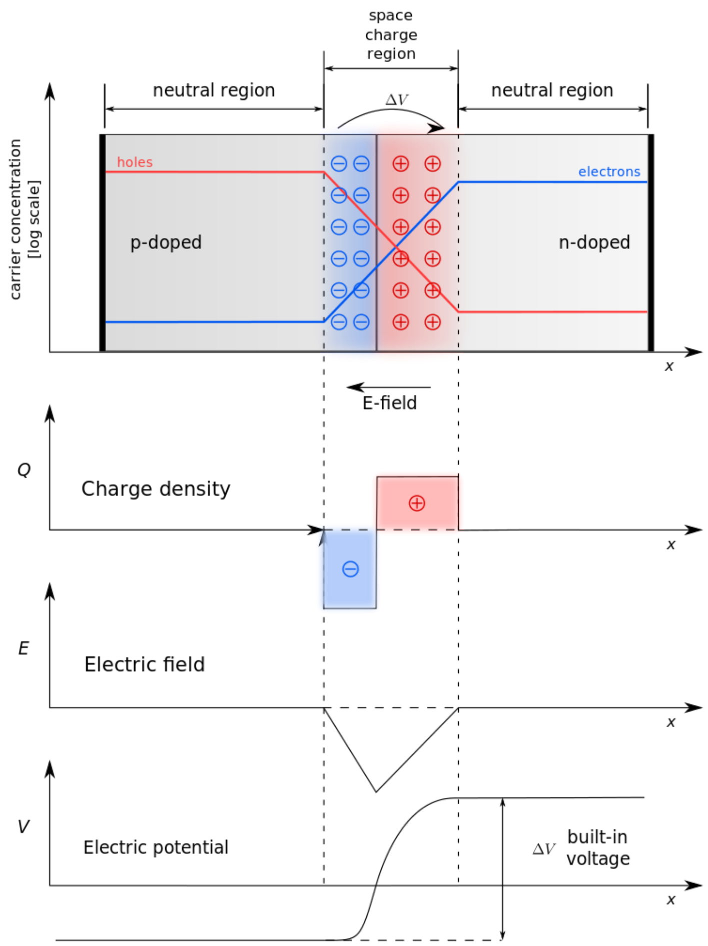

Figure 22: A semiconductor p-n junction with no bias voltage applied. Electrons from the p-type side and holes from the n-type side will distribute in the depletion region in such way, that an electric field will generate. The charge density, the value of the electric field, and the electric potential through the whole junction is shown below [61].

The resulting net current will be lower than in the forward biased junction. Therefore, the p-n junction with applied external electric field acts as a diode, which allows free current flow in one direction and almost no current flow in the other [55].

The semiconductor detectors can be segmented into several detection channels, that can be arranged in a strip or pixel configuration. In the first configuration the channels are put into lines, in the second one they form a matrix. Semiconductor detectors have many advantages. One of the them is the fast operation because the charge carrier formation and collection is much faster than, i.e. in gas-filled detectors. Another advantage is the energy required to generate a charge carrier. For silicon its in order of a few eV, when for a scintillator detector its more than 100 eV. Also, semiconductor detectors have higher energy resolution because of larger amount of charge carriers generated per charged particle flying through the material. Unlike, i.e. scintillators, semiconductor detectors can be produced in compact sizes. In tokamaks, such detectors can be installed in the first wall of the vacuum chamber allowing direct detection of either REs or radiation from the plasma. However, the drawback of these detectors is that they are more

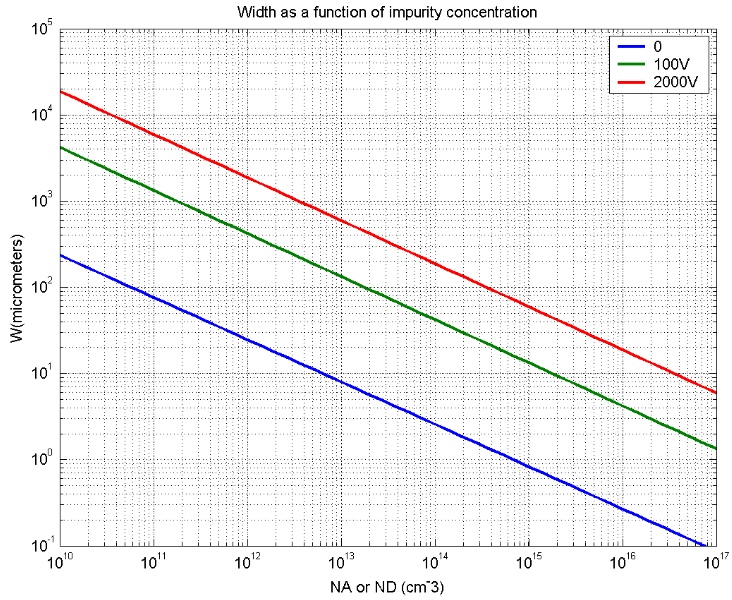

Figure 23: Width of the depletion region dependent on the acceptor or donor atoms concentration and the bias voltage [62].

susceptible to the radiation-induced damage, which brings up a question of shielding and protection of the detector. Another negative factor is the limitation of the small size, as it complicates the detector and electronics arrangement [55], [63].

Strip and pixel detectors allow measurements of position and energy (using time-over-threshold technique, TOT) [63]. The idea behind this arrangement is to divide a p-n diode into many smaller ones. The passing charged particle will create charge carriers in each segment (either strip or pixel), which makes following the particle path possible. The readout system is arranged in such a way, that the signal from each segment is collected separately. More on the strip and pixel detectors can be found in reference [64].

4.2.1 PH32

The PH32 readout is a Si-based semiconductor chip for detection of ionizing particles. It was developed at the Center of Applied Physics and Advanced Detection Systems (CAPADS) at Faculty of Nuclear Science and Physical Engineering, Czech Technical University in Prague in Prague. The chip is arranged into 32 strips with a pitch of 250 μm, the length of each strip is 18 mm. It can operate in two modes: hit counting and energy measurement via TOT. Operation in the high-gain mode allows measurement in the range from 7 keV to 40 keV (SXR and β particles), in the low-gain mode from 37 keV to 5 MeV (α particles and REs). Each strip is connected to a so-called *application specific integrated circuit* (ASIC), which converts an analog signal to a digital. The signal acquisition is done by SURE (Simple USB Readout Equipment), which acts as a data transfer between the chip and operating computer. The PH32 chip has a radiation tolerance suitable for basic spectroscopy [65]. The semiconductor detector with the PH32 chip is shown in Figure 24.

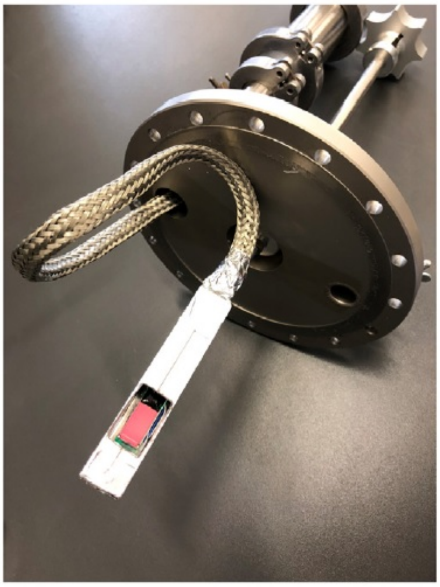

Figure 24: The PH32 detector on a radial manipulator during RE campaign on tokamak GOLEM [63].

4.2.2 X-CHIP-03

The X-CHIP-03 sensor was developed at the Center of Applied Physics and Advanced Detection Systems (CAPADS) at Faculty of Nuclear Science and Physical Engineering, Czech Technical University in Prague for SXR imaging and advanced dosimetry [66]. It is a pixel detector with a matrix of 64×64 pixels with 60 μm pitch. The detector can operate in hit-counting mode and in ADC mode, which allows measurement of the deposited energy. The energy range of operation is from 5 keV to 20 keV. Data acquisition system is presented by a custom readout board FURRy with USB 3.0 interface. First tests were conducted with measuring of X-rays emitted by ^{55}Fe, the results agreed with simulations [66]. The sensor is shown in Figure 25.

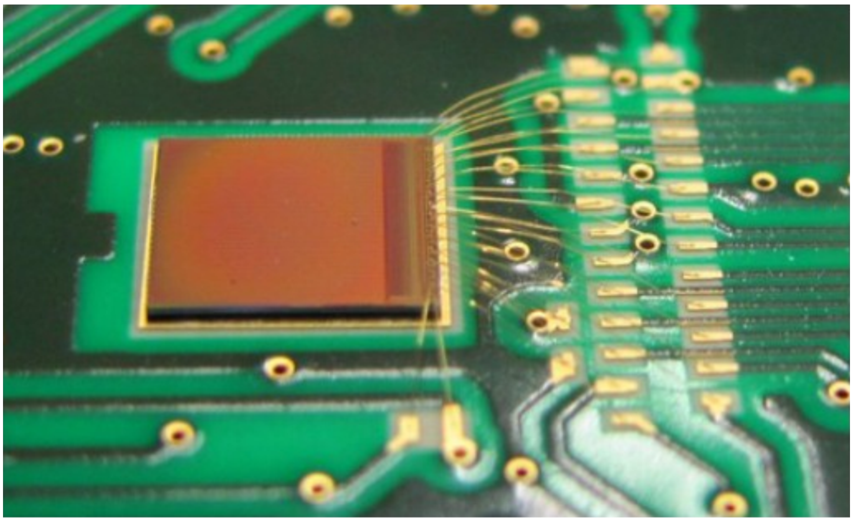

Figure 25: The X-chip-03 detector.

5 Semiconductor detectors in plasma physics

Historically, semiconductor detectors have been used in high energy physics for four decades. However, they have recently found a new application in plasma physics as a novel technique of measurement [63].

5.1 Measurements at tokamak GOLEM

REs generation during the operation of GOLEM tokamak was confirmed via measurements with scintillators [41]. Later, the PH32 chip was tested during RE campaigns.

The first measurements with the PH32 chip were conducted to prove the possibility of direct RE detection using a semiconductor strip detector. The PH32 detector was placed on a radial manipulator inside the tokamak's vessel. Signals from the REs were measured mainly during plasma termination. The acquired data correlated with signals from scintillators (see Figure 26). However, it was shown, that as the detector operates in high electromagnetic field, induced currents in the detector's electronics may lead to either generation of a fake signal or loss of communication between computer and the chip [63].

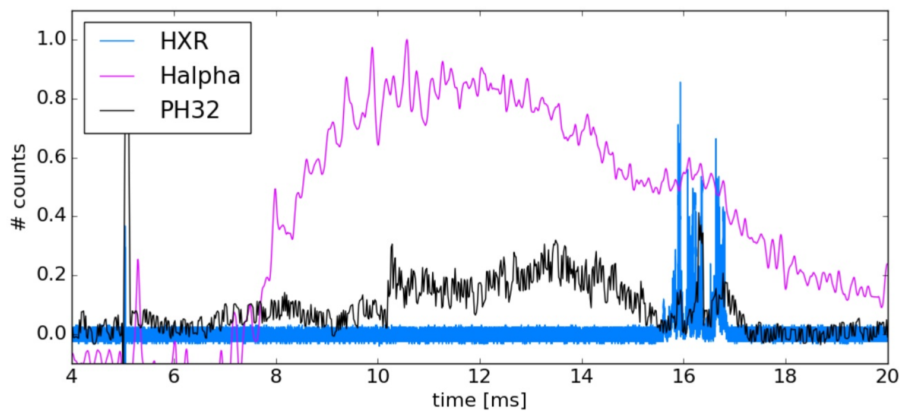

Figure 26: The signal measured by the PH32 chip compared to the signal from scintillator during RE campaign at GOLEM tokamak [63].

Other measurements with the PH32 detector showed saturation of the measured signal (see Figure 27). This proved, that for the detector to operate in the tokamak environment, a better electromagnetic shielding should be provided. The measurements also showed, that the detector setup is not suitable for the direct measurements, as the metal box that shields the detector enters plasma scrape-off layer, while leaving the detector inside the port. This lead to the development of a new detector based on the PH32 readout chip [67].

5.2 Measurements at tokamak COMPASS

The X-chip-03 detector was tested during a RE campaign at tokamak COMPASS. The detector with FURRy readout board was installed at the lower port of the tokamak. Shielding of the electronics was

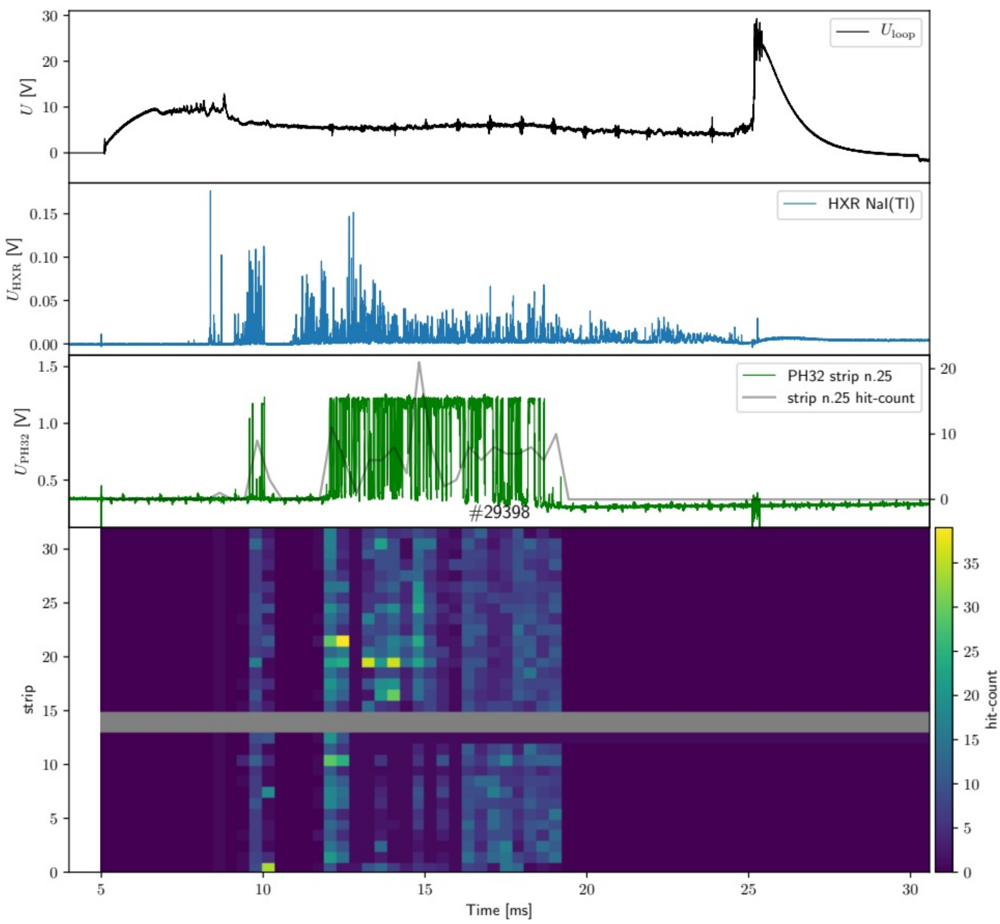

Figure 27: The signal measured by the PH32 chip compared to the signal from scintillator during RE campaign at GOLEM tokamak. Bottom image shows signals detected by each strip over time [67].

provided by a lead pinhole. The setup is shown in Figure 28. Between the detector and the port a beryllium window was installed, which makes it possible to keep the desired vacuum in the tokamak allowing SXR (and electrons with energy ≥ 200 keV) to pass to the detector at the same time. Time between each signal (frame) was set to 10 ms.

To prove, that the signals measured by the detector are generated by electrons, a measurement with ^{90}Sr was conducted. ^{90}Sr is an unstable element with half-life of 28.8 years. It undergoes β^- decay into ^{90}Y. The data from this measurement are shown in Figure 29.

Data from the shot 18971 measured by the detector are show in Figure 30, which is a mean value of the signal from all pixels of the matrix measured in each frame. Length of the RE event is approximately 290 ms. More detailed analysis of the frames 890, 892, and 892 are shown in Figures 31, 32, and 33, respectively. Signals from the frames 890 and 892 are similar to the signal acquired from the measurement with ^{90}Sr (see Figure 29), which means, that these signals are generated by electrons from the plasma. Signal from the frame 891 is saturated.

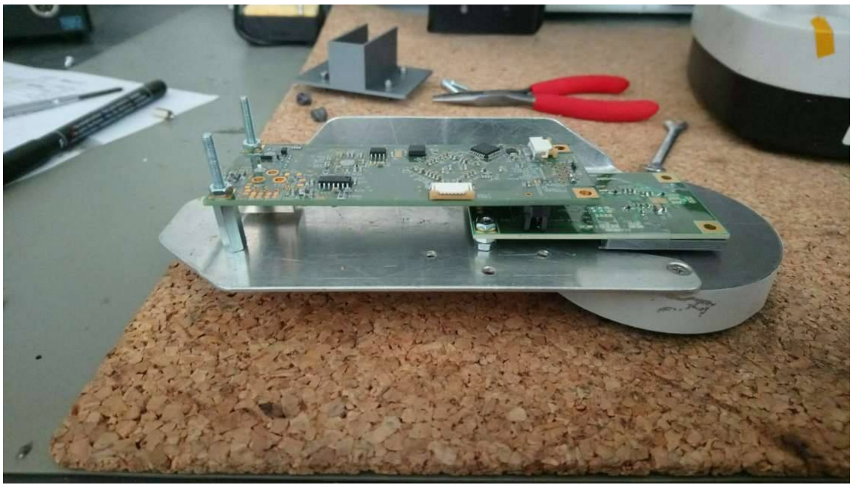

Figure 28: The X-chip-03 detector with FURRy readout board and lead pinhole during RE campaign at tokamak COMPASS.

Signals measured from shots 18969, 18970, 19000, and 19002 are shown in Figure 34, 35, 36, and 37 respectively. Length of the RE event is 170 ms, 190 ms, 600 ms, and 400 ms respectively.

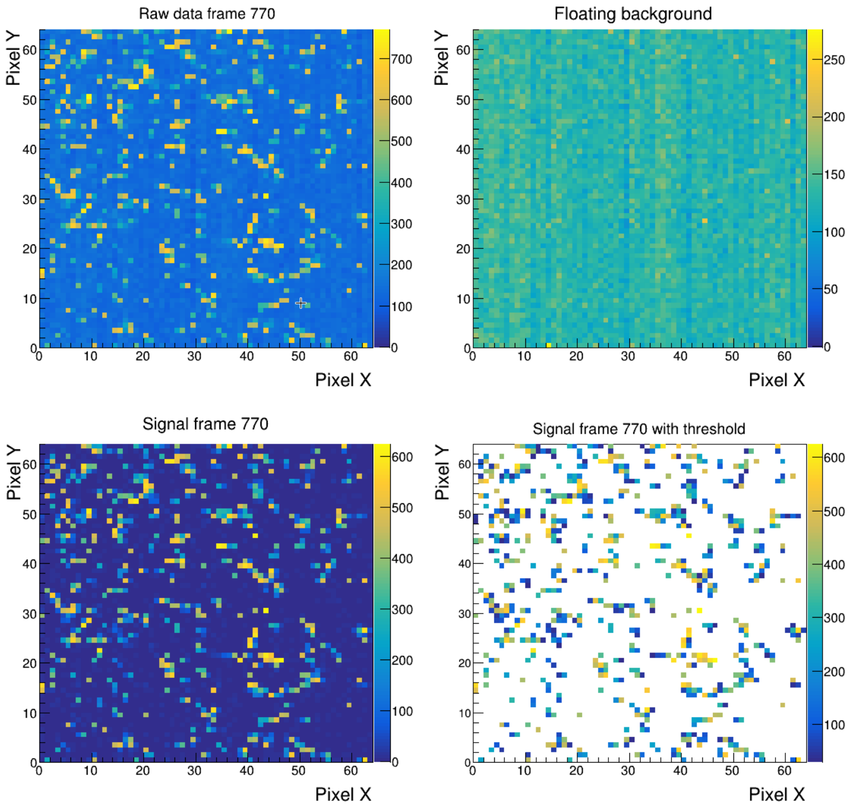

Figure 29: Electrons produced via beta decay of ^{90}Sr measured by the X-chip-03. Top left image is the signal detected, top right is the background signal, bottom left is the signal without background, and bottom right is the signal over threshold of 30 that separates the signal generated by the particles from the noise.

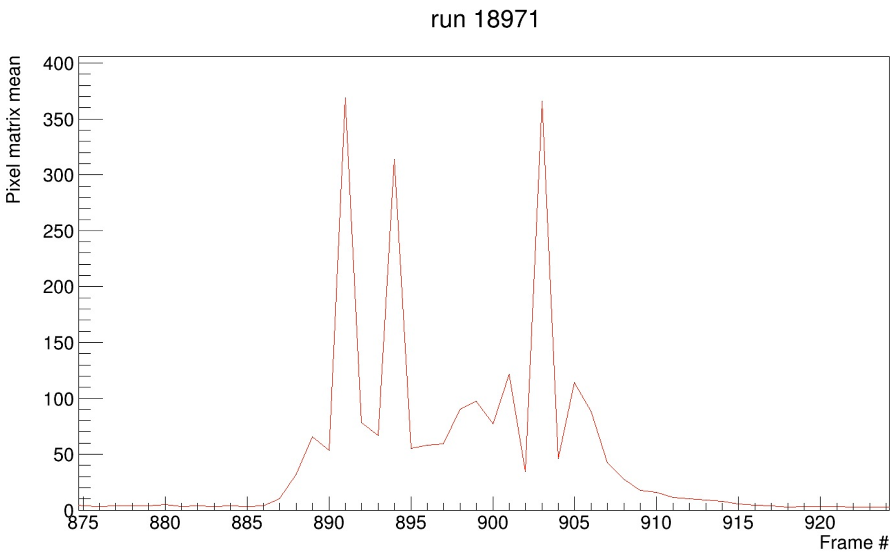

Figure 30: Mean value of the signal measured by all pixels in the matrix of the X-chip-03 detector in shot 18971. Length of the RE event is approximately 290 ms.

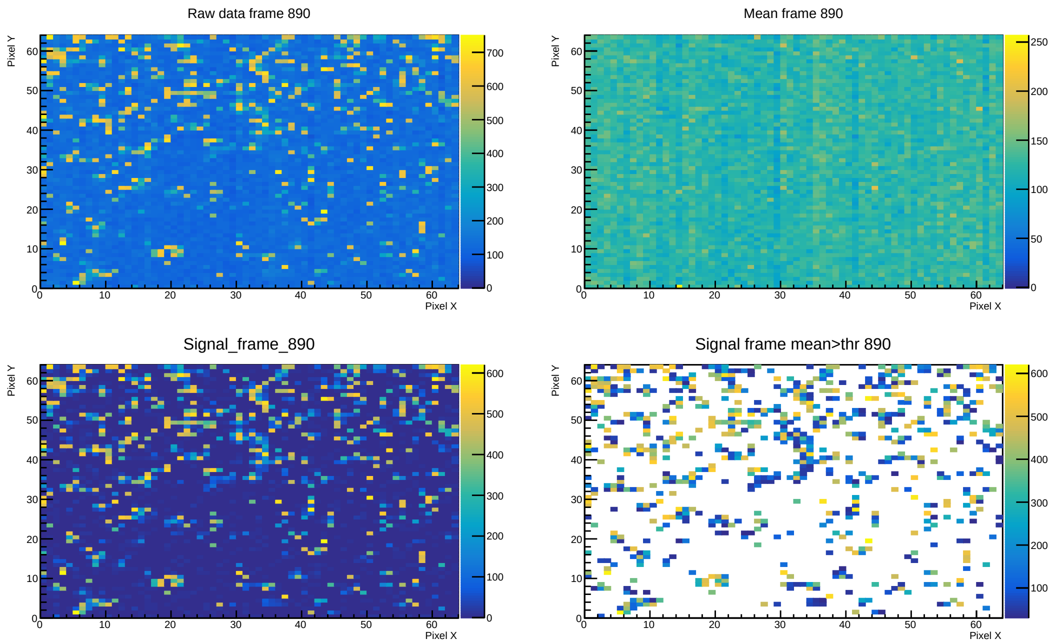

Figure 31: Data acquired by the X-chip-03 detector from shot 18971, frame 890. Top left image is the signal detected, top right is the background signal, bottom left is the signal without background, and bottom right is the signal over threshold of 30 that separates the signal generated by the particles from the noise.

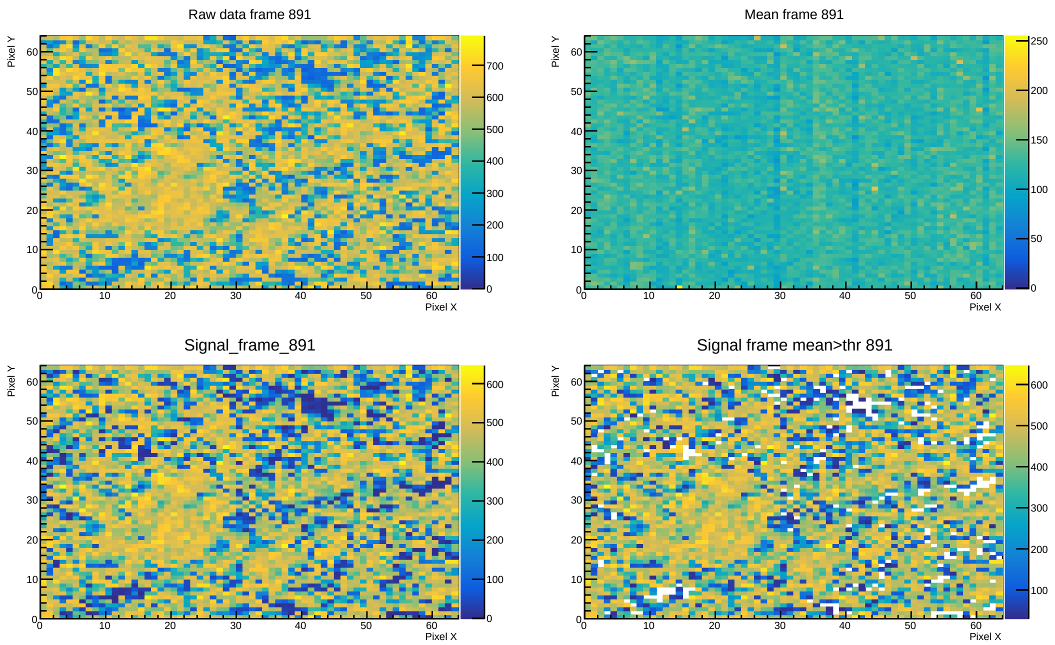

Figure 32: Data acquired by the X-chip-03 detector from shot 18971, frame 891. Top left image is the signal detected, top right is the background signal, bottom left is the signal without background, and bottom right is the signal over threshold of 30 that separates the signal generated by the particles from the noise.

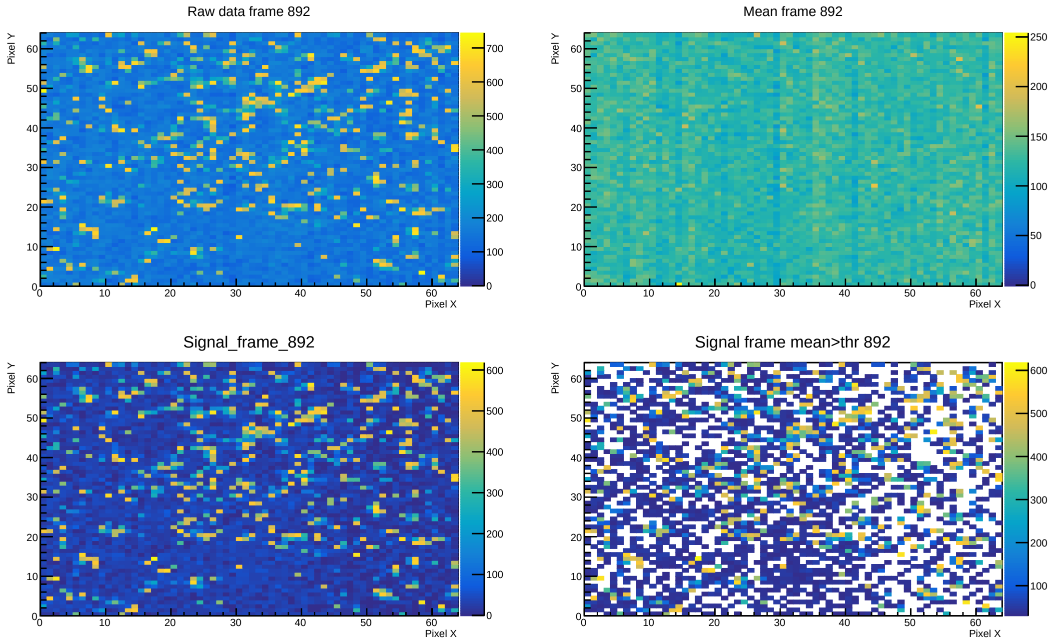

Figure 33: Data acquired by the X-chip-03 detector from shot 18971, frame 892. Top left image is the signal detected, top right is the background signal, bottom left is the signal without background, and bottom right is the signal over threshold of 30 that separates the signal generated by the particles from the noise.

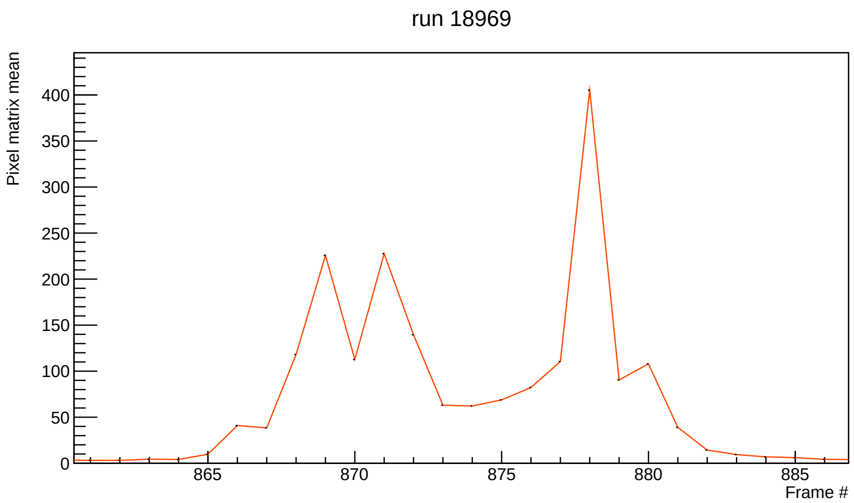

Figure 34: Mean value of the signal measured by all pixels in the matrix of the X-chip-03 detector in shot 18969. Length of the RE event is approximately 170 ms.

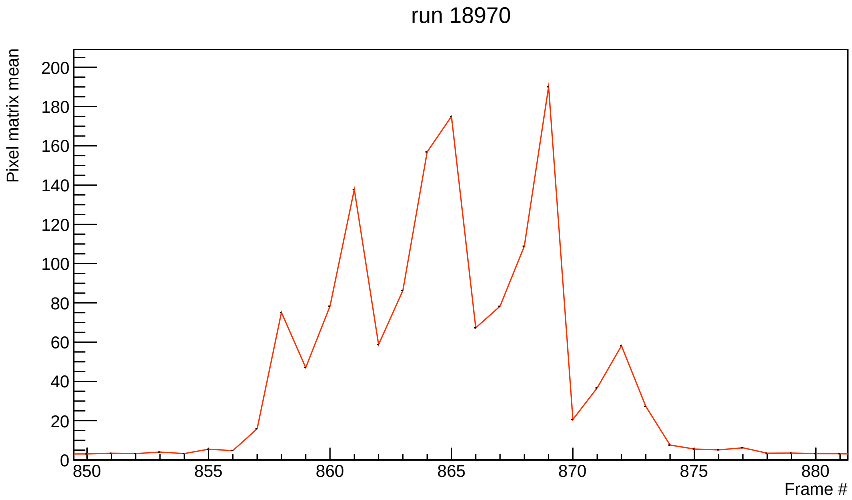

Figure 35: Mean value of the signal measured by all pixels in the matrix of the X-chip-03 detector in shot 18970. Length of the RE event is approximately 190 ms.

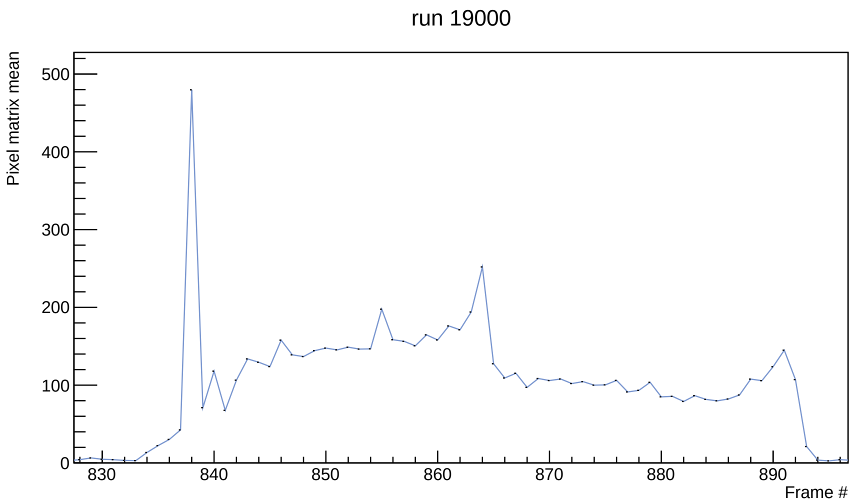

Figure 36: Mean value of the signal measured by all pixels in the matrix of the X-chip-03 detector in shot 19000. Length of the RE event is approximately 600 ms.

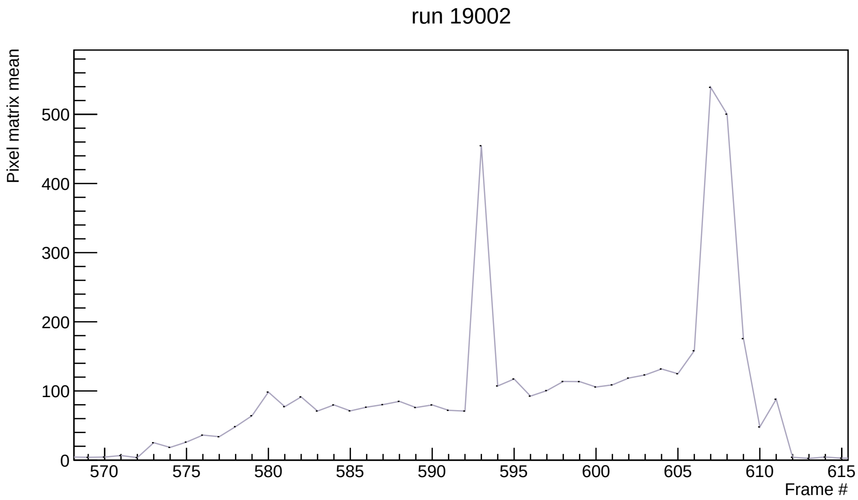

Figure 37: Mean value of the signal measured by all pixels in the matrix of the X-chip-03 detector in shot 19002. Length of the RE event is approximately 400 ms.

Conclusion

Runaway electrons generated during tokamak operation are considered dangerous for the first wall material. The world largest tokamak ITER will have to demonstrate technological and scientific feasibility of thermonuclear fusion enegy. However, REs may not allow to fulfil that goal, as they can shorten the machine's lifetime. To avoid that, new diagnostics methods and mitigation strategies are being developed. Among them are the measurements with detectors based on semiconductor materials, which is a novel technique in plasma physics.

Semiconductor detectors have advantages over other plasma diagnostics, such as the faster operation and lower energy required for the charge carrier generation. The key property of a semiconductor detector is the small size, which makes direct measurements of runaway electrons possible. Semiconductor detectors were used in high energy physics for past four decades. Nonetheless, none of them have been operated in harsh tokamak environment, where high electromagnetic fields, heat and neutron fluxes are detrimental for the detector's electronics.

A silicon strip detector with a PH32 readout chip was tested during RE campaigns at tokamak GOLEM. Experiments have shown, that this detector is useful for the direct measurement of REs inside the tokamak's vessel. However, there are some difficulties that were discovered during the campaigns that have lead to the development of a new detector with a PH32 readout chip with better shielding against high electromagnetic field and more suitable configuration for the in-vessel operation.

The X-chip-03 silicon detector was tested during RE campaigns at tokamak COMPASS. First measurements have shown promising results. Signals measured by the detector were compared with the signals acquired from tests with ^{90}Sr, where signals were generated by the electrons produced during beta decay. The results showed, that the signals measured during RE campaign are generated by the electrons. It is assumed, that these electrons are generated via the Compton scattering of HXR photons on atoms of lead. However, further analysis and comparison with other RE diagnostics installed at tokamak COMPASS is required.

References

[1] J. Mlynář, "Úvod do termojaderné fúze: Fúzní jaderné reakce." https://physics.fjfi.cvut.cz/files/fttf/predmety/02UFU/utf_1_reakce.ppt, Accessed 5.9.2019.

[2] Wikipedia, "Iron-56." https://en.wikipedia.org/wiki/Iron-56, Accessed 8.9.2019.

[3] I. Langmuir, "Oscillations in ionized gases," *Proceedings of the National Academy of Sciences*, vol. 14, no. 8, pp. 627–637, 1928. https://www.pnas.org/content/14/8/627, Accessed 29.8.2019.

[4] P. Kulhanek, "Úvod do teorie plazmatu," 2011. ISBN: 678-80-904582-2-2.

[5] F. F. Chen, "Introduction to plasma physics and controlled fusion," 2016. ISBN: 978-3319223087.

[6] J. Mlynář, "Úvod do termojaderné fúze: Termojaderná fúze ve hvězdách." https://physics.fjfi.cvut.cz/files/fttf/predmety/02UFU/utf_2_hvezdy.ppt, Accessed 5.9.2019.

[7] M. Salaris and S. Cassisi, "Evolution of stars and stellar populations," 2008. ISBN: 978-0470092200.

[8] H. A. Bethe, "Energy production in stars," *Phys. Rev.*, vol. 55, pp. 434–456, Mar 1939. https://link.aps.org/doi/10.1103/PhysRev.55.434, Accessed 27.8.2019.

[9] NobelPrize.org, "The nobel prize in physics 1967," https://www.nobelprize.org/prizes/physics/1967/summary/, Accessed 30.8.2019.

[10] ITER, "External heating." https://www.iter.org/sci/PlasmaHeating, Accessed 27.8.2019.

[11] F. Wagner, "Fusion energy by magnetic confinement," pp. 705–742, 2015. https://onlinelibrary.wiley.com/doi/abs/10.1002/3527600434.eap724, Accessed 1.9.2019.

[12] Y. Xu, "A general comparison between tokamak and stellarator plasmas," *Matter and Radiation at Extremes*, vol. 1, no. 4, pp. 192 – 200, 2016. http://www.sciencedirect.com/science/article/pii/S2468080X16300322, Accessed 1.9.2019.

[13] E. Haug and W. Nakel, "The elementary process of bremsstrahlung," 2004. ISBN: 978-981-238-578-9.

[14] EUROfusion, "Lawson's three criteria," Feb 2013. https://www.euro-fusion.org/news/detail/detail/News/lawsons-three-criteria/, Accessed 29.8.2019.

[15] P.-H. Rebut, "3. european particle accelerator conference," pp. 390–394, 1992. ISBN: 9782863321140.

[16] J. D. Lawson, "Some criteria for a useful thermonuclear reactor," tech. rep., Atomic Energy Research Establishment, 1955.

[17] J. D. Lawson, "Some Criteria for a Power Producing Thermonuclear Reactor," *Proceedings of the Physical Society B*, vol. 70, pp. 6–10, Jan. 1957.

[18] T. Tanabe, "Tritium: fuel of fusion reactors," 2018. ISBN: 978-4-431-56460-7.

[19] J. Mlynář, “Úvod do termojaderné fúze: Kritéria pro užitečný reaktor.” https://physics.fjfi.cvut.cz/files/fttf/predmety/02UFU/utf_3_kriteria.ppt, Accessed 5.9.2019.

[20] R. E. Tipton, “Generalized lawson criteria for inertial confinement fusion,” tech. rep., Lawrence Livermore National Labaratory, 2015.

[21] S. Pfalzner, “An introduction to inertial confinement fusion,” 2006. ISBN: 9780750307017.

[22] M. Kikuchi, “A review of fusion and tokamak research towards steady-state operation: A jaea contribution,” *Energies*, vol. 3, no. 11, p. 1741–1789, 2010.

[23] T. S. Pedersen, R. König, M. Krychowiak, M. Jakubowski, J. Baldzuhn, S. Bozhenkov, G. Fuchert, A. Langenberg, H. Niemann, D. Zhang, and et al., “First results from divertor operation in wendelstein 7-x,” *Plasma Physics and Controlled Fusion*, vol. 61, no. 1, p. 014035, 2018.

[24] Wikipedia, “Tokamak.” https://en.wikipedia.org/wiki/Tokamak, Accessed 8.9.2019.

[25] J. Wesson and D. J. Campbell, “Tokamaks,” 2011. ISBN: 9780199592234.

[26] ITER, “What is iter?.” https://www.iter.org/proj/inafewlines, Accessed 2.9.2019.

[27] ITER, “Broader approach agreement.” https://www.iter.org/sci/iterandbeyond, Accessed 2.9.2019.

[28] ITER, “First plasma: 2025.” https://www.iter.org/mag/9/65, Accessed 1.9.2019.

[29] G. Kalinin, V. Barabash, A. Cardella, J. Dietz, K. Ioki, R. Matera, R. Santoro, and R. Tivey, “Assessment and selection of materials for iter in-vessel components,” *Journal of Nuclear Materials*, vol. 283-287, p. 10–19, 2000.

[30] M. Schaffer, T. Evans, R. Moyer, and M. Fenstermacher, “Elm suppression by resonant magnetic perturbations at diii-d,” *2009 23rd IEEE/NPSS Symposium on Fusion Engineering*, 2009.

[31] R. Kembleton, “Nuclear fusion: What of the future?,” *Managing Global Warming*, p. 199–220, 2019.

[32] “Abundance in earth’s crust of the elements.” https://periodictable.com/Properties/A/CrustAbundance.html, Accessed 3.9.2019.

[33] W. R. Meier, “Tritium breeding management in the high yield lithium injection fusion energy chamber,” *Nuclear Technology*, vol. 52, no. 2, p. 170–178, 1981.

[34] M. Rubel, “Fusion neutrons: Tritium breeding and impact on wall materials and components of diagnostic systems,” *Journal of Fusion Energy*, vol. 38, p. 315–329, Jan 2018.

[35] A. H. Boozer, “Runaway electrons and iter,” *Nuclear Fusion*, vol. 57, no. 5, p. 056018, 2017.

[36] R. Jayakumar, H. Fleischmann, and S. Zweben, “Collisional avalanche exponentiation of run-away electrons in electrified plasmas,” Jan 1992.

[37] I. P. E. G. O. D. Mhd and I. P. B. Editors, “Chapter 3: Mhd stability, operational limits and disruptions,” *Nuclear Fusion*, vol. 39, no. 12, p. 2251–2389, 1999.

[38] B. N. Breizman, P. Aleynikov, E. M. Hollmann, and M. Lehnen, “Physics of runaway electrons in tokamaks,” *Nuclear Fusion*, vol. 59, no. 8, p. 083001, 2019.

[39] N. S. Khaerdinov and A. S. Lidvansky, “Heights of generation of runaway electrons in bright cosmic ray events observed on the ground during thunderstorms,” *Journal of Physics: Conference Series*, vol. 409, p. 012225, Jan 2013.

[40] H. Dreicer, “Electron and ion runaway in a fully ionized gas. ii,” *Physical Review*, vol. 117, no. 2, p. 329–342, 1960. https://doi.org/10.1103/PhysRev.117.329, Accessed 9.9.2019.

[41] O. Ficker, “Generation, losses and detection of runaway electrons in tokamaks,” Master’s thesis, 2015.

[42] J. Connor and R. Hastie, “Relativistic limitations on runaway electrons,” *Nuclear Fusion*, vol. 15, p. 415–424, Jan 1975.

[43] V. Plyusnin, C. Reux, V. Kiptily, G. Pautasso, J. Decker, G. Papp, A. Kallenbach, V. Weinzettl, J. Mlynar, S. Coda, and et al., “Comparison of runaway electron generation parameters in small, medium-sized and large tokamaks—a survey of experiments in compass, tcv, asdex-upgrade and jet,” *Nuclear Fusion*, vol. 58, p. 016014, Aug 2017.

[44] F. C. Schuller, “Disruptions in tokamaks,” *Plasma Physics and Controlled Fusion*, vol. 37, Jan 1995.

[45] H. M. Smith and E. Verwichte, “Hot tail runaway electron generation in tokamak disruptions,” *Physics of Plasmas*, vol. 15, no. 7, p. 072502, 2008.

[46] M. Rosenbluth and S. Putvinski, “Theory for avalanche of runaway electrons in tokamaks,” *Nuclear Fusion*, vol. 37, no. 10, p. 1355–1362, 1997.

[47] S. Drake, “What are the energy range definitions for the various types of electromagnetic radiation?.” https://heasarc.gsfc.nasa.gov/docs/heasarc/headates/spectrum.html Accessed 27.8.2019.

[48] M. Farnik, J. Urban, J. Zajac, O. Bogar, O. Ficker, E. Macusova, J. Mlynar, J. Cerovsky, M. Varavin, V. Weinzettl, and et al., “Runaway electron diagnostics for the compass tokamak using ec emission,” *EPJ Web of Conferences*, vol. 203, p. 03006, 2019.

[49] C. Liu, L. Shi, E. Hirvijoki, D. P. Brennan, A. Bhattacharjee, C. Paz-Soldan, and M. E. Austin, “The effects of kinetic instabilities on the electron cyclotron emission from runaway electrons,” *Nuclear Fusion*, vol. 58, p. 096030, Dec 2018.

[50] Wikipedia, “Scintillation counter.” https://en.wikipedia.org/wiki/Scintillation_counter, Accessed 9.9.2019.

[51] M. Forster, K. H. Finken, M. Lehnen, O. Willi, and Y. a. Xu, “Measurements of the runaway electron energy during disruptions in the tokamak textor,” *Physics of Plasmas*, vol. 19, no. 5, p. 052506, 2012.

[52] L. Baylor, C. C. Barbier, J. R. Carmichael, S. K. Combs, M. N. Ericson, N. D. B. Ezell, P. W. Fisher, M. S. Lyttle, S. J. Meitner, D. A. Rasmussen, and et al., “Disruption mitigation system developments and design for iter,” *Fusion Science and Technology*, vol. 68, no. 2, p. 211–215, 2015.

[53] N. Commaux, L. Baylor, T. Jernigan, E. Hollmann, P. Parks, D. Humphreys, J. Wesley, and J. Yu, "Demonstration of rapid shutdown using large shattered deuterium pellet injection in diii-d," *Nuclear Fusion*, vol. 50, p. 112001, Aug 2010.

[54] M. Lehnen, G. Arnoux, S. Brezinsek, J. Flanagan, S. Gerasimov, N. Hartmann, T. Hender, A. Huber, S. Jachmich, V. Kiptily, and et al., "Impact and mitigation of disruptions with the iter-like wall in jet," *Nuclear Fusion*, vol. 53, p. 093007, Sep 2013.

[55] G. F. Knoll, "Radiation detection and measurement," 2000. ISBN: 0-471-07338-5.

[56] L. L. Gunderson and J. E. Tepper, "Clinical radiation oncology," 2015. ISBN: 978-0323240987.

[57] R. N. J. Cherry, "Chapter 48 - radiation: Ionizing." `http://www.ilocis.org/documents/chpt48e.htm`, Accessed 5.9.2019.

[58] NIST, "Cross-section for the photon-silicon interaction." `https://physics.nist.gov/PhysRefData/Xcom/html/xcom1.html`, Accessed 9.9.2019.

[59] F. Gallmeier, "General purpose photoneutron production in mcnp4a," 1995. `https://www.osti.gov/biblio/207563-general-purpose-photoneutron-production-mcnp4a`, Accessed 5.9.2019.

[60] A. Rogalski, "Infrared detectors," 2011. ISBN: 9781420076714.

[61] Wikipedia, "p-n junction." `https://en.wikipedia.org/wiki/P\T1\textendashn_junction`, Accessed 9.9.2019.

[62] Wikipedia, "Depletion region." `https://en.wikipedia.org/wiki/Depletion_region`, Accessed 11.9.2019.

[63] P. Svihra, D. Bren, A. Casolari, J. Cerovsky, P. Dhyani, M. Farnik, O. Ficker, M. Havranek, M. Hejtmanek, Z. Janoska, and et al., "Runaway electrons diagnostics using segmented semiconductor detectors," *Fusion Engineering and Design*, vol. 146, p. 316–319, 2019.

[64] G. Lutz, "Semiconductor radiation detectors: device physics," 2007. ISBN: 978-3-540-71679-2.

[65] Z. Janoska, M. Carna, M. Havranek, M. Hejtmanek, V. Kafka, M. Marcisovsky, G. Neue, L. Tomasek, and V. Vrba, "Measurement of ionizing particles by the ph32 chip," *2015 IEEE Nuclear Science Symposium and Medical Imaging Conference (NSS/MIC)*, 2015.

[66] M. Havranek, T. Benka, M. Hejtmanek, Z. Janoska, D. Lednicky, V. Kafka, M. Marcisovska, M. Marcisovsky, G. Neue, P. Svihra, and et al., "X-chip-03: Soi maps radiation sensor with hit-counting and adc mode," *2018 IEEE Nuclear Science Symposium and Medical Imaging Conference Proceedings (NSS/MIC)*, 2018.

[67] M. Tunkl, D. Bren, P. Dhyani, M. Farnik, O. Ficker, M. Havranek, M. Hejtmanek, Z. Janoska, V. Kafka, S. Kulkov, M. Marcisovska, M. Marcisovsky, J. Mlynar, G. Neue, L. Novotny, P. Svihra, V. Svoboda, L. Tomasek, and V. Vrba, "The direct detection of runaway electrons using the semiconductor strip detector," *46th EPS Conference on Plasma Physics*, 2019.